Latest Miocene-earliest Pliocene evolution of the ancestral Rio Grande at the Española-San Luis Basin boundary, northern New Mexico

D.J. Koning, S. Aby, V.J.S Grauch, and M.J. Zimmerer

New Mexico Geology, v. 38, n. 2 pp. 24-49, Online ISSN: 2837-6420.
https://doi.org/10.58799/NMG-v38n2.24

This page is intentionally left blank to maintain order of facing pages.

Latest Miocene-earliest Pliocene evolution of the ancestral Rio Grande at the Española-San Luis Basin boundary, northern New Mexico

Daniel J. Koning[1], Scott Aby[2], V.J.S. Grauch[3], Matthew J. Zimmerer[1]
[1] New Mexico Bureau of Geology and Mineral Resources, New Mexico Institute of Mining and Technology, 801 Leroy Place, Socorro, NM, 87801, USA; *dkoning@nmbg.nmt.edu*
[2] Muddy Spring Geology, P.O. Box 488, Dixon, NM 87527, USA
[3] U.S. Geological Survey, MS 964, Federal Center, Denver, CO, 80225, USA

Abstract

We use stratigraphic relations, paleoflow data, and $^{40}Ar/^{39}Ar$ dating to interpret net aggradation, punctuated by at least two minor incisional events, along part of the upper ancestral Rio Grande fluvial system between 5.5 and 4.5 Ma (in northern New Mexico). The studied fluvial deposits, which we informally call the Sandlin unit of the Santa Fe Group, overlie a structural high between the San Luis and Española Basins. The Sandlin unit was deposited by two merging, west- to southwest-flowing, ancestral Rio Grande tributaries respectively sourced in the central Taos Mountains and southern Taos Mountains-northeastern Picuris Mountains. The river confluence progressively shifted southwestward (downstream) with time, and the integrated river (ancestral Rio Grande) flowed southwards into the Española Basin to merge with the ancestral Rio Chama. Just prior to the end of the Miocene, this fluvial system was incised in the southern part of the study area (resulting in an approximately 4–7 km wide paleovalley), and had sufficient competency to transport cobbles and boulders. Sometime between emplacement of two basalt flows dated at 5.54±0.38 Ma and 4.82±0.20 Ma (groundmass $^{40}Ar/^{39}Ar$ ages), this fluvial system deposited 10–12 m of sandier sediment (lower Sandlin subunit) preserved in the northern part of this paleovalley. The fluvial system widened between 4.82±0.20 and 4.50±0.07 Ma, depositing coarse sand and fine gravel up to 14 km north of the present-day Rio Grande. This 10–25 m-thick sediment package (upper Sandlin unit) buried earlier south- to southeast-trending paleovalleys (500–800 m wide) inferred from aeromagnetic data. Two brief incisional events are recognized. The first was caused by the 4.82±0.20 Ma basalt flow impounding south-flowing paleodrainages, and the second occurred shortly after emplacement of a 4.69±0.09 Ma basalt flow in the northern study area. Drivers responsible for Sandlin unit aggradation may include climate-modulated hydrologic factors (i.e., variable sediment supply and water discharge) or a reduction of eastward tilt rates of the southern San Luis Basin half graben. If regional in extent, these phenomena could also have promoted fluvial spillover that occurred in the southern Albuquerque Basin at about 6–5 Ma, resulting in southward expansion of the Rio Grande to southern New Mexico.

Introduction

An intriguing event in the history of the Rio Grande rift, occurring in the latest Miocene or earliest Pliocene, was a remarkable downstream elongation of the Rio Grande from the Albuquerque Basin southward to southern New Mexico, where it alternately avulsed into several playa-lake systems (Mack et al., 1997 and 2006; Connell et al., 2005). This southward expansion resulted in the fluvial integration of several previously closed basins in south-central New Mexico. Previous studies in the Socorro and Palomas Basins bracket the age of this integration between ~6 and 4.6 Ma (Chamberlin, 1999; Chamberlin et al., 2001; Mack et al., 1998 and 2006; Koning et al., 2015, 2016a). Workers have suggested this downstream-directed integration occurred because of 1) orogenic-enhanced precipitation due to rift-flank uplift of mountains in the late Miocene (Chapin and Cather, 1994), 2) fluvial spillover because of reduced subsidence rates in rift basins (Cather et al., 1994; Connell et al., 2005), 3) fluvial spillover due to paleoclimatic changes affecting water vs. sediment discharges (Kottlowski, 1953; Chapin, 2008; Connell et al., 2012), or 4) epeirogenic doming and mantle-driven uplift (Kottlowski, 1953; Repasch, 2015a, b). Note that this southward expansion of the Rio Grande occurred prior to the 0.43 Ma integration of Lake Alamosa in the northern San Luis Basin (Machette et al., 2013).

As a step in understanding the downstream elongation of the ancestral Rio Grande, this study explores episodes of aggradation and incision that occurred in the latest Miocene-earliest Pliocene at the boundary between the Española and San Luis Basins (Fig. 1). There, we describe a gravelly sand deposited by two merging Rio Grande tributaries that drained the southern San Luis Basin. The river below this merger, which we define as the ancestral Rio Grande due to its geographic similarity to the modern Rio Grande and coarser texture of its sediment compared to underlying (late Miocene) deposits, flowed southwestward and joined with the ancestral Rio Chama in the middle to southern Española Basin (Koning and Aby, 2005; Koning et al., 2016b). This axial river then flowed into the northern Santo Domingo Basin, where a Rio Chama-dominated axial-fluvial system was established by 6.96 Ma (Smith et al., 2001; Smith, 2004). Whether the northern of these tributaries was fluvially connected with the northern San Luis Basin in the latest Miocene-earliest Pliocene is not known. If the ancestral Rio Grande only drained the southern San Luis Basin, then the Rio Chama (modern drainage area of 8,142 km2; U.S. Geological Survey, 2009) would have been the larger tributary at this time. Note that we use the term "river" in a broad sense to convey a geographically large fluvial system (e.g., having a drainage area >500 km^2) that may be ephemeral, consistent with modern geographic usage in New Mexico of "river" and its Spanish variant, "rio."

The studied fluvial sediment is locally underlain and overlain by four basalt flows whose $^{40}Ar/^{39}Ar$ ages (from groundmass) bracket the unit between 5.5–4.5 Ma.

We synthesize these ages with stratigraphic relations and aeromagnetic data to interpret a basic chronologic sequence of latest Miocene erosion, net aggradation between 5.5 and 4.5 Ma punctuated by episodic incision, followed by erosion. Complexities in this sequence of events are described below. Finally, we briefly discuss the implications of this fluvial history to the concomitant downstream elongation of the Rio Grande.

Geologic Setting

The study area is located on the western margin of the southernmost Taos Plateau, overlying a structural high between the San Luis and Española Basins of the northern Rio Grande rift (Fig. 1). This structural high is manifested by a northwest-trending Bouguer gravity high (Cordell, 1979; Manley, 1979a; Ferguson et al., 1995; Koning et al.,

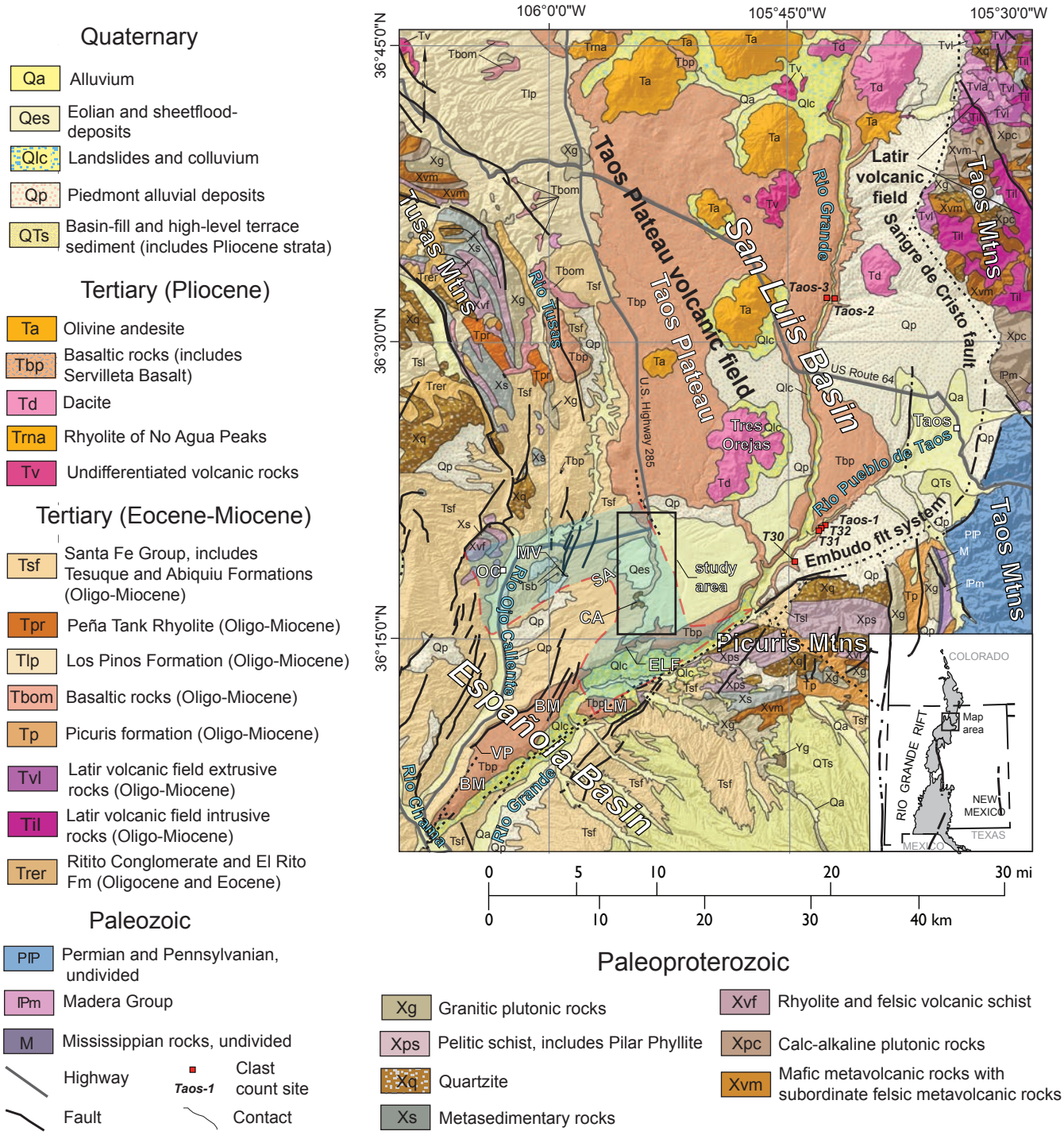

Figure 1. Geologic map of the southern San Luis Basin and northern Española Basin. Study area indicated by the black, rectangular box. The location of the inter-basin structural high is shaded a light bluish-green color bounded by a dashed red line in the lower left of the figure; this area coincides with positive isostatic residual gravity values from Grauch and Keller (2004). Site abbreviations: BM=Black Mesa; CA=Cerro Azul; MV=Mesa Vibora; ELF=Embudo local fauna site of Aby and Morgan (2011); LM=La Mesita; OC=Ojo Caliente; SA=Sandlin Arroyo; VP=Vallito Peak. Usage of Servilleta Basalt follows terminology of Lipman and Mehnert (1979), Abiquiu Formation and Ritito Conglomerate is used as defined by Maldonado and Kelley (2009), and usage of Picuris formation follows Rehder (1986) and Aby et al. (2004). Geologic map is modified from Koning and Mansell (2011), who in turn updated the 1:500,000 geologic map of New Mexico (NMBGMR, 2003).

2004a) and local outcrops of Proterozoic bedrock (Kelley, 1978; Koning et al., 2007a). Bounding the southeast side of this structural high is the left-lateral Embudo fault, which transfers extensional strain between the San Luis and Española Basins (Muehlberger, 1978, 1979; Kelson et al., 2004; Koning et al., 2004a). A component of northwest-down throw along the Embudo fault permitted minor sediment accumulation on the structural high adjacent to the fault.

The Taos Plateau occupies the southern San Luis Basin (Fig. 1) and is underlain by a succession of more than 210 m of Pliocene-age fluvial sediment and interlayered basalt flows. The southern San Luis Basin coincides with an east-tilted graben, whose master fault system (the Sangre de Cristo fault) has tilted Pliocene strata gently to the east and south (Bauer and Kelson, 2004). The package of Pliocene basalt and sediment has commonly been referred to as the Servilleta Formation (Butler, 1946, 1971; Montgomery, 1953; Lambert, 1966; Galusha and Blick, 1971; Drakos et al., 2004), but some workers prefer to use separate names for the basalts vs. sediment (e.g., Lipman and Mehnert, 1979; Dungan et al., 1984). In this paper, we follow the latter convention and use Servilleta Basalt (Lipman and Mehnert, 1979). The Servilleta Basalt is part of the Taos Plateau volcanic field, which also includes minor andesite, basaltic andesite, and dacite flows (Ozima et al., 1967; Lipman and Mehnert, 1979; Thompson and McMillan, 1992).

Numerous studies have investigated the geochronology of the basaltic rocks of the Taos Plateau volcanic field. Reported ages of the basalts range from 4.8 to 2.5 Ma (Ozima et al., 1967; Lipman and Mehnert, 1979; Baldridge et al., 1980; Appelt, 1998). Within this time span, Dungan et al. (1984) interpret three short-lived episodes of volcanism (compared to inter-eruptive time intervals) based on three major geochemical varieties of basalts separated by gravelly sediment. But $^{40}Ar/^{39}Ar$ dating of 86 lava samples (using primarily groundmass) indicates a relatively regular temporal spacing of basaltic volcanism (Appelt et al., 1998). Repasch et al. (2015a, b) present a 4.5 Ma basalt age from Black Mesa, which they use to interpret the presence of the ancestral Rio Grande by that time.

In the southern San Luis Basin, pre-Servilleta Basalt basin-fill stratigraphy has been studied using data from sparse, deep water-supply wells (e.g., Drakos et al., 2004). Correlative basin-fill strata to the south have received much study in the well-exposed Española Basin, which serves as the type area for the Santa Fe Group (Spiegel and Baldwin, 1963; Galusha and Blick, 1971). In the northern Española Basin, the upper Santa Fe Group consists of a fluviatile package called the Chamita Formation overlying an eolian unit called the Ojo Caliente Sandstone Member of the Tesuque Formation. The Vallito Member of the Chamita Formation (defined by Koning and Aby, 2005), is particularly relevant for our study and interpreted to represent deposition from a sandy, bedload-dominated fluvial system draining the southern San Luis Basin during late Miocene time (Koning and Aby, 2005). Previous mapping by several workers illustrate the stratigraphy and structure of the Santa Fe Group within 20 km south and southwest of the study area (Manley, 1976, 1979b; May, 1980; Steinpress, 1981; Koning and Aby, 2003; Koning and Manley, 2003; Koning, 2004; Koning et al., 2004b).

Our study describes scattered exposures along a 12-km long escarpment, south of U.S. Highway 285, that coincides with the west side of the southern Taos Plateau. A prominent landmark in the study area is Cerro Azul, a steep-sided, 170-m tall hill that abuts the southwestern end of the Taos Plateau. The top of the Taos Plateau rises 30–60 m above gentle, rolling topography in the northern Española Basin to the west. Immediately south of the study area, the Embudo local fauna (ELF) site lies at the south end of the Taos Plateau (Fig. 1). There, a Blancan (4.9–1.6 Ma) fossil assemblage was found at the top of a 12–15 m thick, fining-upward interval of sand and gravel that unconformably overlies the Ojo Caliente Sandstone (Aby and Morgan, 2011).

Methods

Descriptions and differentiation of distinctive Santa Fe units were conducted as part of geologic mapping (Koning and Aby, 2003; Koning et al., 2007a). In addition, three stratigraphic sections were measured. Gravel counts and paleoflow measurements were made at the stratigraphic sections and elsewhere in the mapped area. Paleoflow directions were determined by measuring clast imbrication (n=129) and channel-margin trends (n=3).

High-resolution aeromagnetic data were interpreted after application of a reduction-to-pole transformation (Bankey et al., 2007) that corrects for shifts of anomalies away from the centers of their magnetic sources. The approach to interpreting remanent magnetization of volcanic rocks from aeromagnetic data follows that of Grauch et al. (2004, 2006) and Grauch and Keller (2004).

Basaltic groundmass from three lava flows and one crystallized lava lake were dated using the $^{40}Ar/^{39}Ar$ technique. Sample preparation included crushing, sieving, washing away clay-sized material in deionized water, dissolving carbonate with hydrochloric acid, and removing phenocrysts using a Frantz magnetic separator and optical picking under a binocular microscope. The groundmass separates and the 28.201 Ma Fish Canyon interlaboratory standard (Kuiper et al., 2008) were loaded into aluminum discs and irradiated at the US Geological Survey TRIGA reactor in Denver. Analyses were completed at the New Mexico Geochronology Research Laboratory. Samples were incrementally heated and released gases were cleaned by a getter pump in an all-metal, fully automated extraction line. Isotopic ratios were measured using a MAP 215-50 mass spectrometer. More information regarding the $^{40}Ar/^{39}Ar$ technique can be found in McIntosh et al. (2003). Data tables and additional analytical parameters are in Appendix 1 (Data Repository 20160002).
http://geoinfo.nmt.edu/repository/index.cfml?rid=20160002

Lithologic units

Stratigraphic nomenclature

At least three informal names have been applied to Pliocene-Pleistocene clastic deposits elsewhere in the San Luis Basin: the Lama formation (Pazzaglia and Wells, 1990), Blueberry Hill deposit (Bauer and Kelson, 1997; Kelson et al., 2001; Bauer et al., 2004), and the Servilleta Formation (Butler, 1946, 1971; Montgomery, 1953; Lambert, 1966). Until the Pliocene sediment in the

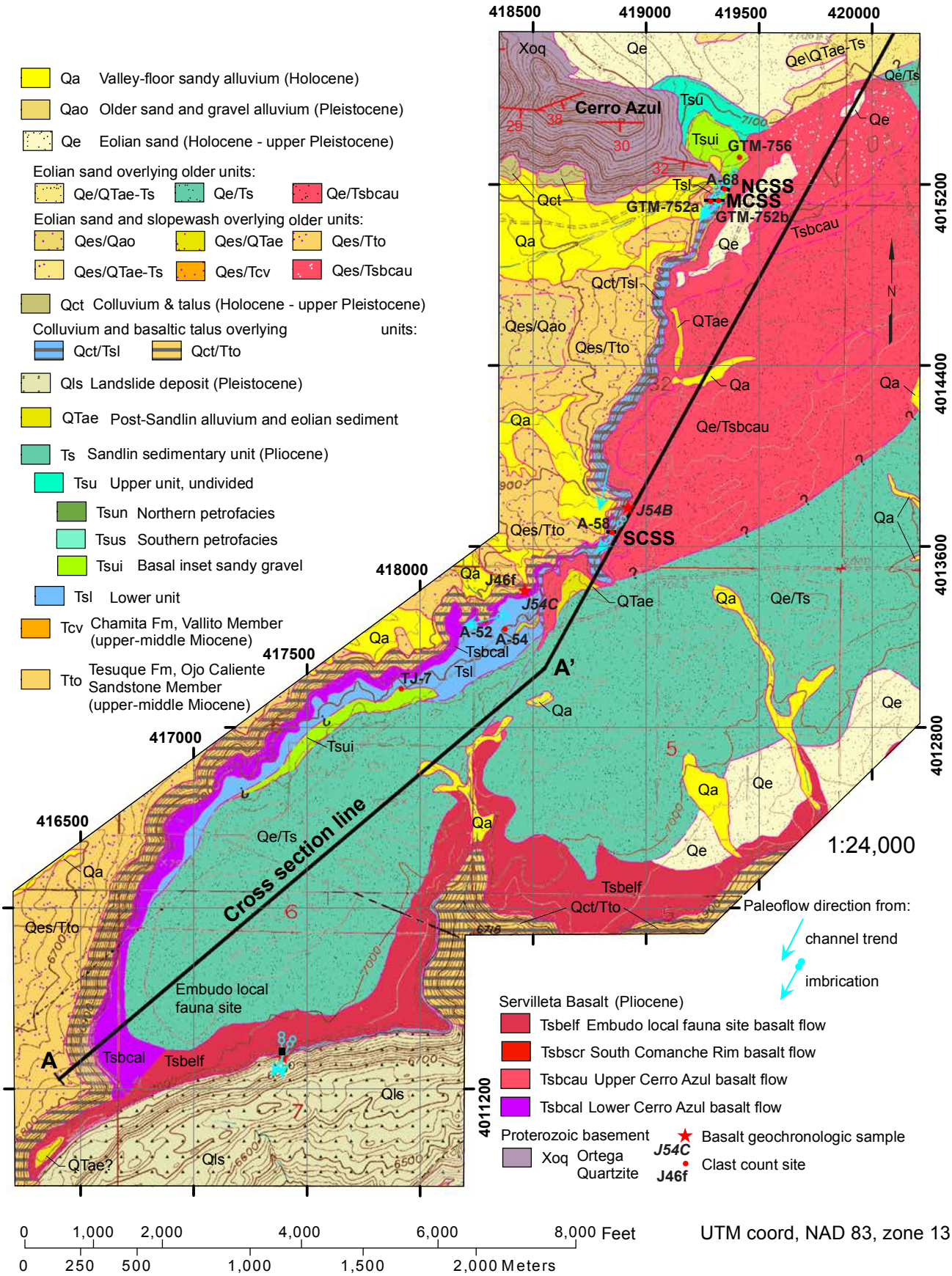

Figure 2. Geologic map of the southern half of the study area. Contour interval is 20 feet. Paleoflow data are from Appendix 6 and Koning et al. (2007a). The thick black line depicts the location of the vertically exaggerated cross section of A-A''' (Figure 4). SCSS, MCSS, and NCSS = south, middle and north Cerro Azul stratigraphic sections, respectively. Usage of Vallito Member (Chamita Formation) follows definition of Koning and Aby (2005); usage of Servilleta Basalt follows terminology of Lipman and Mehnert (1979).

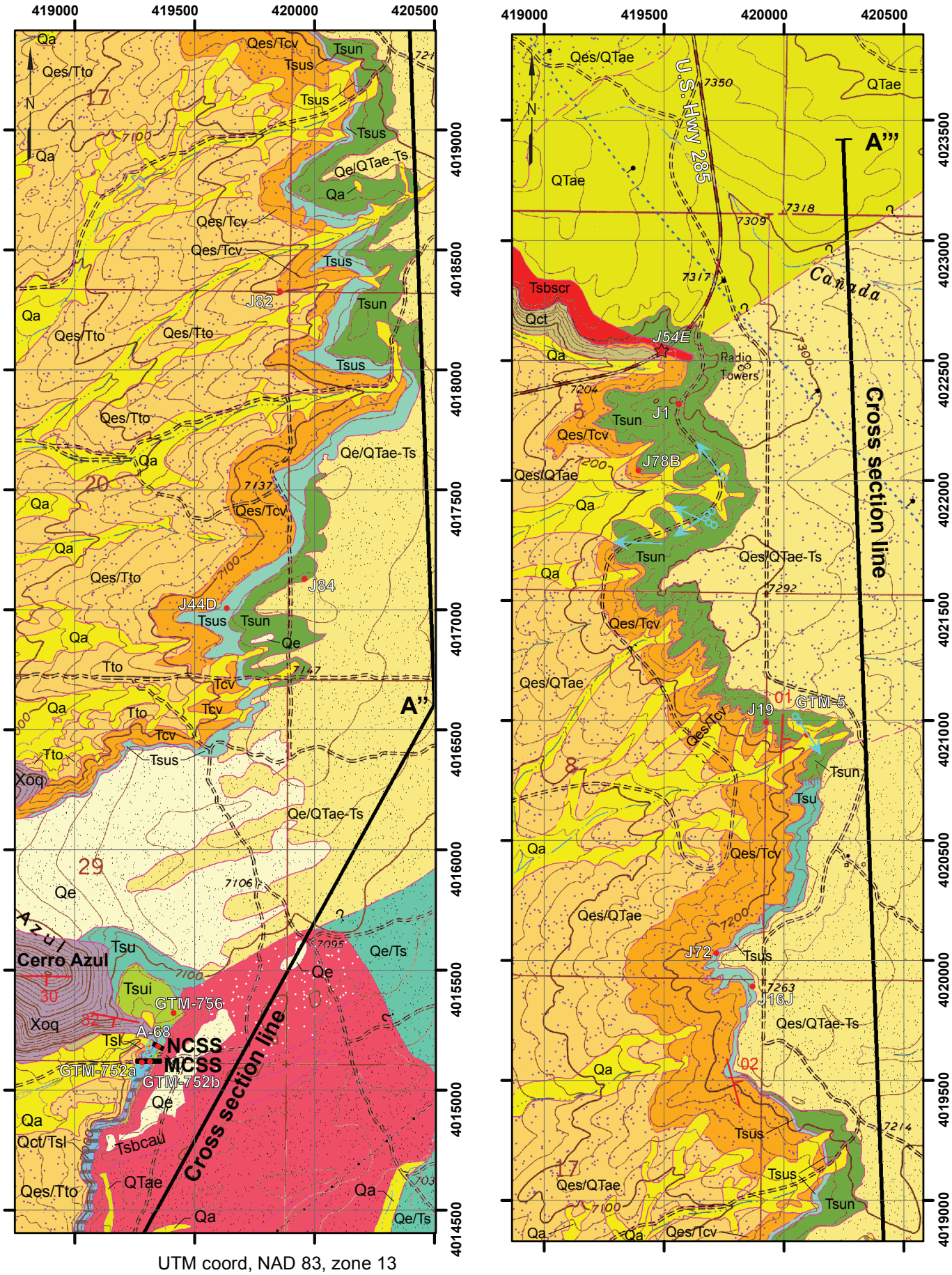

Figure 3. Geologic map of the middle and northern parts of the study area (left and right panels, respectively). See Figure 2 for explanation of map units. Contour interval is 20 feet. The thick black line depicts the location of the vertically exaggerated cross section of A-A''' (Figure 4).

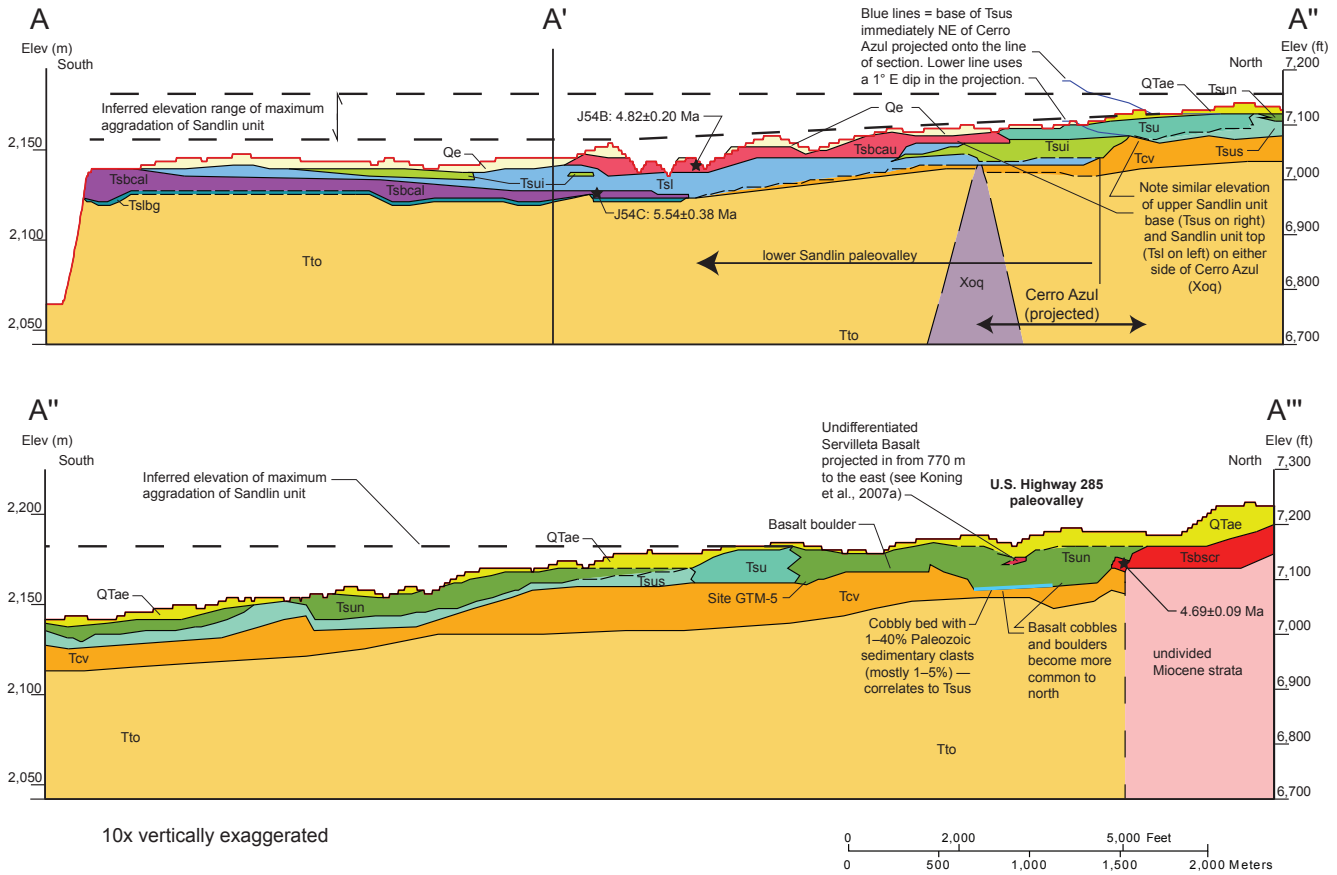

Figure 4. Vertically exaggerated, north-south cross-section showing stratigraphic relations in study area. Cross-section line depicted as A-A''' in Figures 2–3. In A''-A''', all lithologic contacts are projected onto the line of section using a 1°E apparent dip. See Figure 2 for explanation of unit labels.

southern San Luis Basin is formally assigned a name with an appropriate type section, we informally and provisionally refer to the predominantly Pliocene deposits in the study area as the Sandlin unit of the Santa Fe Group, named after a nearby drainage to the west (Fig. 1).

The Sandlin unit can be divided into upper and lower subunits based on the elevation of the deposit and stratigraphic position relative to the upper basalt flow near Cerro Azul (Figs. 2–4), which we informally call the upper Cerro Azul flow and describe below. The elevation of the lower Sandlin subunit progressively decreases from 7,030–7,080 ft (2,143–2,158 m), at the southeast corner of Cerro Azul, southwards to 6,960–7,020 ft (2,121–2,140 m) at the southern end of Taos Plateau; it is capped by the upper Cerro Azul flow. The elevation range of the exposed upper Sandlin subunit increases in an irregular fashion from 7,080–7,180 ft (2,158–2,188 m), at Cerro Azul, northwards to 7,270–7,310 ft (2,216–2,228 m) near U.S. Highway 285; it is not overlain by the upper Cerro Azul flow. Within the upper Sandlin subunit, two gravel-based petrofacies are differentiated (Figs. 2–4) and described below.

The Chamita and Tesuque Formations (Santa Fe Group) underlie the Sandlin unit (Figs. 2–4). The sandy sediment of the Chamita Formation is correlated to the Vallito Member based on lithologic similarity (Koning and Aby, 2005)—particularly its predominant fine- to medium-grained sand texture, common slightly orangish color, and clast composition—but exposure does not permit direct physical correlation. Locally, the Vallito Member along the escarpment has sparse very fine to medium pebbles composed of rhyolitic lavas and tuffs, greenish Paleozoic sedimentary clasts, dacite, quartzite, and granite (most to least abundant). The tan, cross-stratified sandstone of the Tesuque Formation corresponds to the Ojo Caliente Sandstone Member (Galusha and Blick, 1971; May, 1980). Detailed descriptions of these strata are given in Appendix 2.

We correlate three stratigraphically distinctive mafic flows in the study area to the Servilleta Basalt (Figs. 2–4). All three flows contain olivine phenocrysts, supporting a field-based designation of "basalt." The northern basalt underlies the northernmost Sandlin unit near U.S. Highway 285 and continues northward along the Comanche Rim. For the purposes of this study, we informally call it the south Comanche Rim flow (Tsbscr). The other two basalts are found south of Cerro Azul. These are informally referred to as the lower and upper Cerro Azul basalt flows (Tsbcal and Tsbcau) based on their proximity to Cerro Azul.

Key gravel types

We found gravel composition to be very useful in interpreting provenance. To match clast types to potential source areas, we studied previous geologic mapping of highlands surrounding the southern San Luis Basin and conducted gravel counts of near-source Pliocene deposits deemed representative of three general source areas (Table 1; Fig. 5): Arroyo Hondo (representing the north-central Picuris

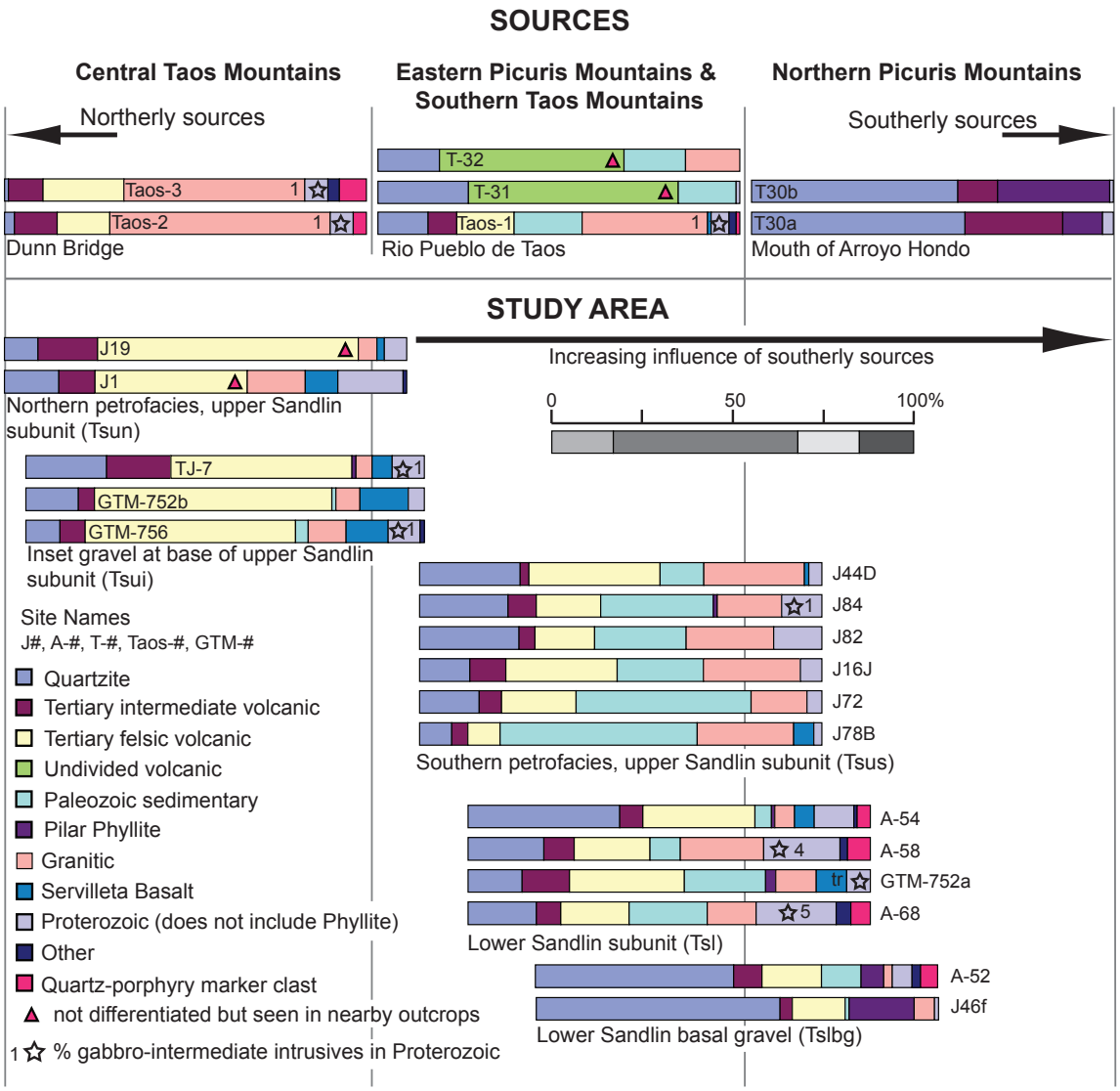

Figure 5. Bar graphs illustrating the results of clast counts near potential source areas (top) and in the study area (bottom). Graphs are grouped according to subunit (following Table 2). Horizontal placement of the subunits reflects inferred relative contributions from the source areas listed above. Note that northerly source areas in the study area also include gravel recycling from the Tusas Mountains–Taos Plateau border region (not reflected in the near-source clast counts).

Mountains; site T30), Rio Pueblo de Taos (representing the northeastern Picuris Mountains and southern Taos Mountains; sites Taos-1, T31, and T32), and near Dunn Bridge in the Rio Grande Gorge (representing the central Taos Mountains; sites Taos-2 and Taos-3).

Four gravel types are particularly important for identifying basin-fill provenance (Figs. 5–6). The first gravel type consists of greenish-brownish sedimentary rocks composed of sandstone, siltstone, and limestone, the latter being much less abundant than the other types (Fig. 6A)

These lithologies match quartzose to feldspathic Paleozoic sedimentary rocks restricted to the southern Taos Mountains, east and southeast of Taos (unit PP of Fig. 1; Montgomery, 1953; Bauer, 1993; Bauer and Kelson, 1997; Kelson and Bauer, 1998; Bauer et al., 2000; Kelson et al., 2001); hereafter we refer to this gravel suite as "Paleozoic sedimentary clasts." These clasts differ from reworked Santa Fe Group sandstone clasts, which typically are composed of either volcaniclastic sandstone or white-tan, subrounded sandstone of the Ojo Caliente Sandstone Member of the Tesuque Formation.

Two other useful clast types for determining provenance include the Pilar Phyllite and a quartz-bearing porphyry that we informally call the "quartz-porphyry marker clast." The Pilar Phyllite (Fig. 6B) is a gray-black, carbonaceous, quartz-muscovite phyllite with slaty cleavage. It is restricted to the Picuris Mountains (unit Xps of Fig. 1; Montgomery, 1953; Bauer, 1993; Bauer and Kelson, 1997; Kelson and Bauer, 1998), consistent with being observed in the Arroyo Hondo near-source clast count sites but not those farther to the north (Table 1).

The quartz-porphyry marker clast is a durable rhyolite that commonly becomes slightly polished during transport (Fig. 6C–E). Its color ranges from light gray, light yellow, or light greenish yellow. The clast's phenocryst assemblage is dominated by quartz and contains ≤1% sanidine and ≤1% mafic minerals. The

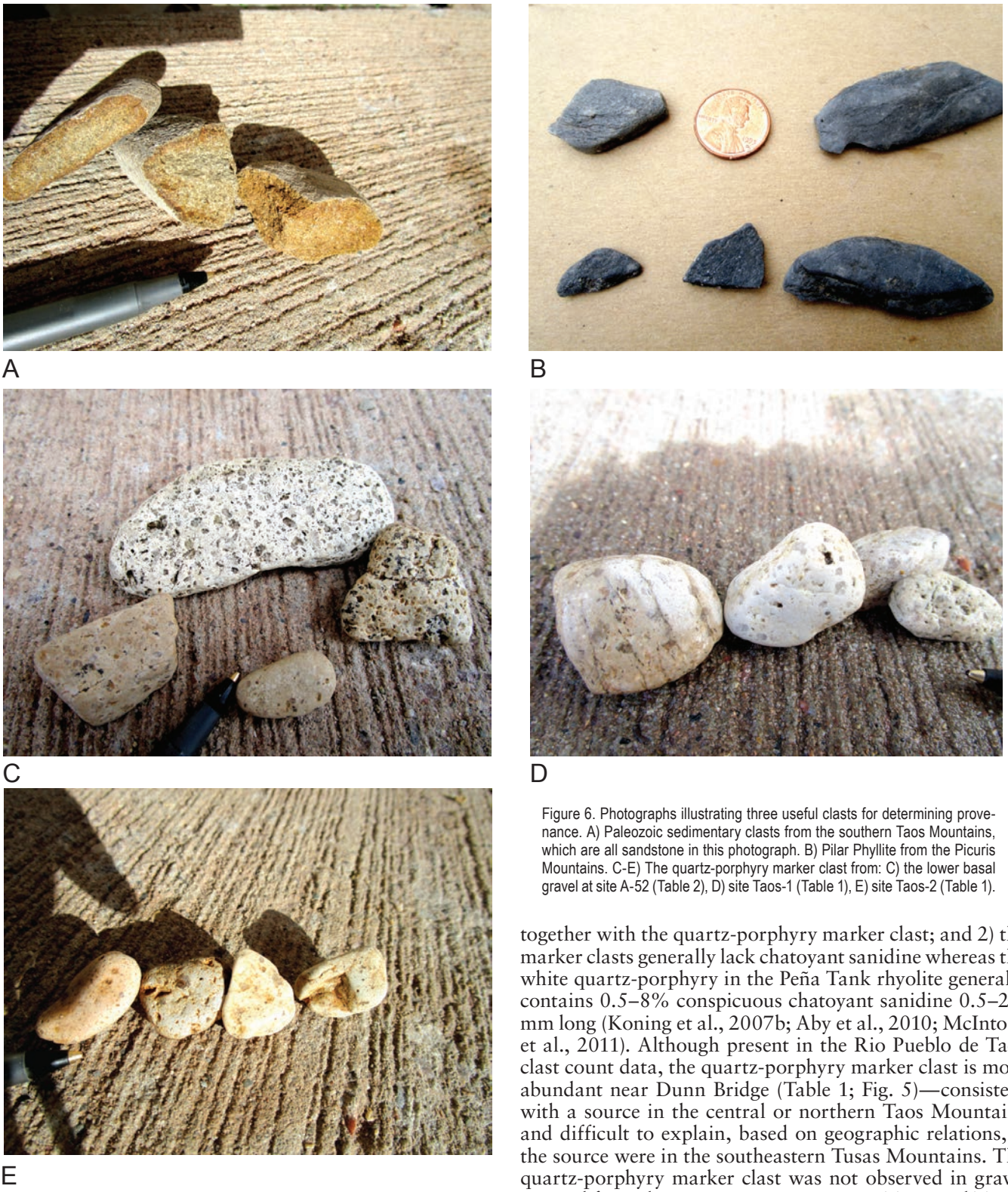

Figure 6. Photographs illustrating three useful clasts for determining provenance. A) Paleozoic sedimentary clasts from the southern Taos Mountains, which are all sandstone in this photograph. B) Pilar Phyllite from the Picuris Mountains. C-E) The quartz-porphyry marker clast from: C) the lower basal gravel at site A-52 (Table 2), D) site Taos-1 (Table 1), E) site Taos-2 (Table 1).

quartz-porphyry marker clast is likely derived from a silicic unit in the Latir volcanic field in the central Taos Mountains (Lipman et al., 1986), but the specific intrusion, ignimbrite, or flow has not been identified. Quartz porphyries have not been observed in the Picuris Mountains or southern Taos Mountains. The quartz-porphyry marker clast cannot be derived from the white quartz-porphyry observed in the Peña Tank Rhyolite (unit Tpr, Fig. 1) in the southeastern Tusas Mountains because: 1) the red-gray lithologic types of the Peña Tank Rhyolite are not observed together with the quartz-porphyry marker clast; and 2) the marker clasts generally lack chatoyant sanidine whereas the white quartz-porphyry in the Peña Tank rhyolite generally contains 0.5–8% conspicuous chatoyant sanidine 0.5–2.0 mm long (Koning et al., 2007b; Aby et al., 2010; McIntosh et al., 2011). Although present in the Rio Pueblo de Taos clast count data, the quartz-porphyry marker clast is more abundant near Dunn Bridge (Table 1; Fig. 5)—consistent with a source in the central or northern Taos Mountains and difficult to explain, based on geographic relations, if the source were in the southeastern Tusas Mountains. The quartz-porphyry marker clast was not observed in gravel sourced from the Picuris Mountains (sites T30a and T30b, Table 1; Fig. 5).

Gravel composed of gabbroic and intermediate intrusives (inferred to be granodiorite, quartz diorite, or diorite based on hand sample identification) are best correlated with the central Taos Mountains. Gabbroic and intermediate intrusives in the central Taos Mountains include: granodiorite of Jaracito Canyon, tonalite of Red River, and undivided mafic-ultramafic rocks (Lipman and Reed, 1989); note that these are included in unit Xpc on Fig. 1. In near-source clast count data, slightly more

TABLE 1. Clast count data from Pliocene sedimentary deposits east-northeast of study area

Site:	T30a	T30b	Taos-1	T-31	T-32	Taos-2	Taos-3
Location:	Mouth of Arroyo Hondo	Mouth of Arroyo Hondo	Rio Pueblo de Taos	Rio Pueblo de Taos	Rio Pueblo de Taos	Rio Grande at Dunn Bridge	Rio Grande at Dunn Bridge
Provenance:	North-central Picuris Mtns	North-central Picuris Mtns	S Taos Mtns, NE Picuris Mtns	S Taos Mtns, NE Picuris Mtns	S Taos Mtns, NE Picuris Mtns	Central Taos Mtns	Central Taos Mtns
Quartzite	59%	57%	14%	25%	17%	3%	1%
Tertiary intermediate volcanic*			8%			13%	9%
Tertiary felsic volcanic*			16%			16%	21%
Volcanic (undivided)]	27%	11%	24%	58%	51%	29%	4%
Paleozic sedimentary	0%	0%	19%	16%	17%	0%	0%
Vein quartz	0%	0%	3%	0%	0%	1%	2%
Proterozoic amphibolite	0%	0%	0%	0%	0%	1%	1%
Pilar Phyllite	11%	31%	0%	0%	0%	0%	0%
Non-foliated granitic**	0%	0%	16%			40%	39%
Foliated granitic**	0%	0%	19%			16%	8%
Granite (undivided)	0%	0%	35%	0%	15%	67%	47%
Servilleta Basalt	0%	0%	1%	0%	0%	0%	0%
Proterozoic schist	3%	1%	0%	1%	0%	0%	0%
Gabbro-intermediate intrusives	0%	0%	1%***	0%	0%	1%	1%
Mylonite	0%	0%	1%			4%	2%
Other	0%	0%	2%	0%	0%	0%	3%
Quartz-porphyry*	0%	0%	1%			4%	7%
Comments:			Other = chlorite-rich intrusive, epidote-rich intrusive				Other = 1 epidote-rich intrusive; 2 Fe-rich rocks
Easting^	432949	432969	435670	435291	435779	436773	436316
Northing^	4019449	4019454	4022633	4022399	4022643	4043635	4043401

Note: * This clast type was subsumed into "Tertiary volcanics (undivided)" where shaded.
** This clast type was subsumed into "Granite (undivided)" where shaded.
*** The gabbro may possibly be amphibolite.
^ UTM coordinates in meters; datum is NAD83 (zone 13).

gabbro-diorite is seen near Dunn Bridge than the Rio Pueblo de Taos, and none are observed at Arroyo Hondo (Table 1; Fig. 5).

Other gravel types cannot be attributed to a single-source locality. For example, volcanic gravel is found in the central Taos Mountains, Picuris Mountains, and the Tusas Mountains–Taos Plateau border region (i.e., the Cordito Member of the Los Pinos Formation; Manley, 1981). The original eruptive center for this gravel was likely the Latir volcanic field, but erosion and fluvial activity in the late Oligocene through Miocene has transported the volcanic gravel to the west and south. Granitoids, quartzites, vein quartz, and amphibolites are found in both the Picuris Mountains and central Taos Mountains (Fig. 1; Montgomery, 1953; Lipman and Reed, 1989; Bauer, 1993). Granitic rocks are also found in the Tusas Mountains–Taos Plateau border region (e.g., Tres Piedras granite of Just (1937) and Barker (1958)).

Stratigraphic relations

Figures 2 and 3 present an updated version of previous geologic mapping (i.e., Koning and Aby, 2003; Koning et al., 2007a). A north-south, vertically exaggerated cross-section illustrates stratigraphic relations found in the study area (Fig. 4), as do three stratigraphic sections in the southern study area (Fig. 7, Appendix 3) whose locations are depicted in Figure 2. Sandlin strata dip gently east-southeast (≤1.0°) north of Cerro Azul and appear to be subhorizontal to the south, based on kilometer-scale cross-section relations and attitudes measured primarily by three-point procedures from the geologic map (Figs. 2–4). Bedding attitudes of the underlying Chamita Formation are subhorizontal or dip up to 2° E. The basal contact of the Sandlin unit is scoured, where exposed, and map and cross-section relations suggest irregular relief over 10^2-10^3 m horizontal distances, consistent with erosional topography (Figs. 2–4).

Three stratigraphic relations in the 10–25 m thick upper Sandlin subunit are noteworthy. One, in cross-section A-A'' east of Cerro Azul, the basal contact of the upper Sandlin subunit projects to a similar elevation as the upper contact of the lower Sandlin subunit (Fig. 4). Two, the northern petrofacies of the Sandlin subunit progrades southward over the southern petrofacies north of Cerro Azul. Three, in the north part of our study area, in the vicinity of U.S. Highway 285, the upper Sandlin subunit thickens in a 700-m wide paleovalley we informally name the U.S. Highway 285 paleovalley (Fig. 4). Locally, the basal 1–2 m of the upper Sandlin subunit in this paleovalley is cobbly and contains 1–40% Paleozoic sedimentary clasts as well as minor basalt boulders (Appendix 4). The basal gravel of the U.S. Highway 285 paleovalley is inset ~8 m beneath the base of the south Comanche Rim flow (Tsbscr). On the north side of the paleovalley, stratigraphically higher strata of the upper Sandlin subunit onlaps the south Comanche Rim basalt flow (Fig. 4).

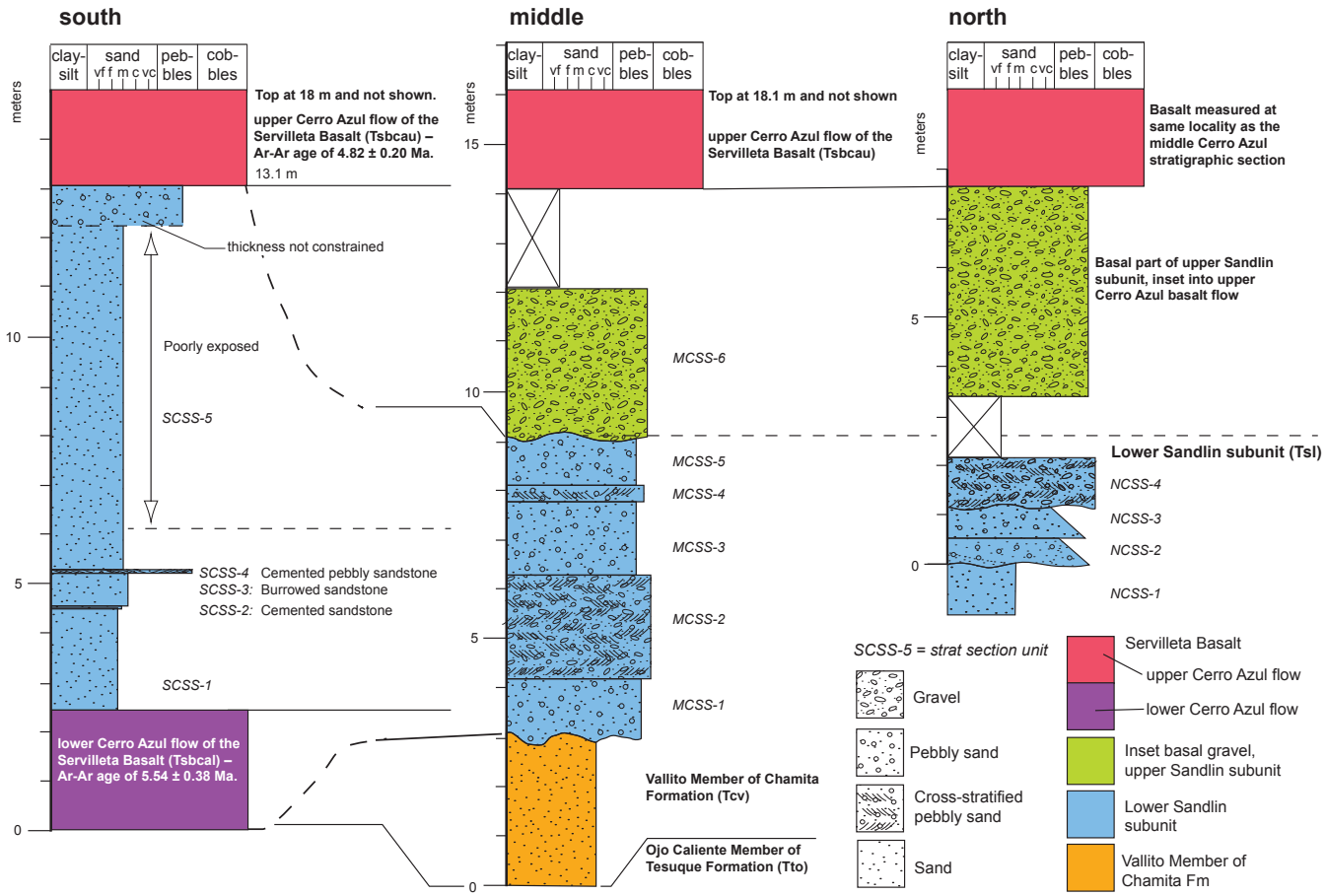

Figure 7. Cerro Azul stratigraphic sections. Locations depicted in Figures 2 and 3. Thicknesses of the south Cerro Azul section and pre-basaltic strata of the north Cerro Azul section were measured using eye height and a Brunton compass, but subunit thicknesses of the exposed lower Sandlin unit in the north Cerro Azul section were double-checked with a ruler. The middle Cerro Azul section was measured using an Abney level and Jacob's staff.

Stratigraphic relations between the lower Sandlin subunit and Servilleta Basalt flows are important to our interpretations (Figs 2, 4, 6). Two exposures reveal 1.0–1.5 m of cobble- and boulder-bearing gravel beneath the lower Cerro Azul flow, which we call the basal gravel of the lower Sandlin subunit (Fig. 8). Located between the lower and upper Cerro Azul flows is a 10–12 m-thick interval of sand with minor gravel that we assign to the lower Sandlin subunit (Fig. 7).

Immediately east of Cerro Azul, a volcanic-rich gravel appears to conformably underlie the bulk of the upper Sandlin subunit (Tsui, Figs. 3–4). Southeast of Cerro Azul, this gravel is inset ~5 m below the base of the upper Cerro Azul basalt flow. This inset relation is demonstrated by meter-scale boulders of basalt associated with this gravel, one of which is clearly part of a cemented fluvial deposit (Fig. 9). These boulders match the olivine-phyric basalt of the upper Cerro

Azul flow. Therefore, the gravel must postdate this flow and we include this gravel with the upper Sandlin subunit.

The Sandlin unit appears to overlie unique Miocene Santa Fe Group units north and south of Cerro Azul. To the north of this landmark, the Vallito Member of the Chamita Formation underlies the Sandlin unit. To the south of Cerro Azul, the Ojo Caliente Sandstone (Tesuque Formation) underlies the Sandlin unit and the lower Cerro Azul basalt flow. The only exception to this generalization is found immediately southeast of Cerro Azul, where 3 m thickness of the Vallito Member is preserved in the lower Cerro Azul stratigraphic section above the Ojo Caliente Sandstone (Figs. 7, 10). Previous work suggests an age range of 10 to 6(?) Ma for the Vallito Member and 13.2 to 9 Ma for the Ojo Caliente Sandstone in the northern Española Basin (Koning et al., 2011, 2013), but no direct age control is available in the study area. Thus, the Vallito Member appears to have been largely eroded south of Cerro Azul prior to Sandlin deposition. It is possible that the Vallito Member north of Cerro Azul is time-correlative with the lower Sandlin unit to the south. If true, this relation requires an abrupt facies change across Cerro Azul. However, a buttress unconformity between the two units is implied by the abruptness of the observed facies change, by the coincidence of the northward termination of subunit Tsui with this inferred buttress, and a noteworthy northward thickening (from 3 to 30 m) of the Vallito Member (Figs. 3–4).

The Sandlin unit is overlain by younger Pliocene-Pleistocene sand (unit QTae of Koning et al., 2007a), which is described in Appendix 2. The contact between this sand and the underlying Sandlin unit is difficult to map due to poor exposure, but the exact position of the contact is not critical to our study.

Sandlin Unit

Description

The Sandlin unit is composed of sand and gravelly sand representing stacked channel fills (Fig. 10). It differs from the underlying Chamita Formation by its coarser texture (both in the sand and gravel fractions) and overall browner color, versus a common slightly orangish color in the Chamita Formation. Below, we summarize descriptions from our stratigraphic sections (Fig. 7, Appendix 3) and Koning et al. (2007a, where equivalent strata are mapped as Tats and Tatn). The sandy lower Sandlin subunit is light gray

Figure 8. Photograph of sandy gravel underlying the informal lower Cerro Azul basalt (5.54 ± 0.38 Ma), which is 1.5 m thick at this locality. This is the oldest known deposit of cobble- and boulder-bearing gravel of the ancestral Rio Grande in the area. The gravel is particularly rich in quartzite and contains 6% Pilar Phyllite (site A-52, Table 2). The lack of basalt gravel indicates deposition prior to emplacement of the Servilleta Basalt. Pen for scale just above the contact with underlying, light-tan sand of the Ojo Caliente Sandstone Member (Tesuque Formation). Photograph taken at UTM coordinates (NAD 83): 418285 m E, 4013270 m N.

A

B

Figure 9. Photographs of basaltic boulders associated with the basal, inset gravel of the upper Sandlin unit (Tsui) southeast of Cerro Azul. These boulders have relatively coarse olivine phenocrysts similar to the informal upper Cerro Azul basalt flow, and are as large as 3 m at clast count site TJ-7 (Table 2). The lithologic similarity to the upper Cerro Azul basalt flow, together with the large boulder sizes, supports our inset interpretation. A) Basalt boulder cemented together with pebbly sand of the Sandlin unit. The pebbles here are subangular and composed of quartzite and felsic volcanics along with 10% Paleozoic sandstone, 1% intermediate intrusive with epidote, 1–3% granitoids, and 1% quartz-porphyry marker clasts (percentages from visual estimation). Hammer for scale. B) Meter-scale boulders of basalt that look similar to the upper Cerro Azul basalt are weathering out of the inset gravel near clast count site A-54.

A

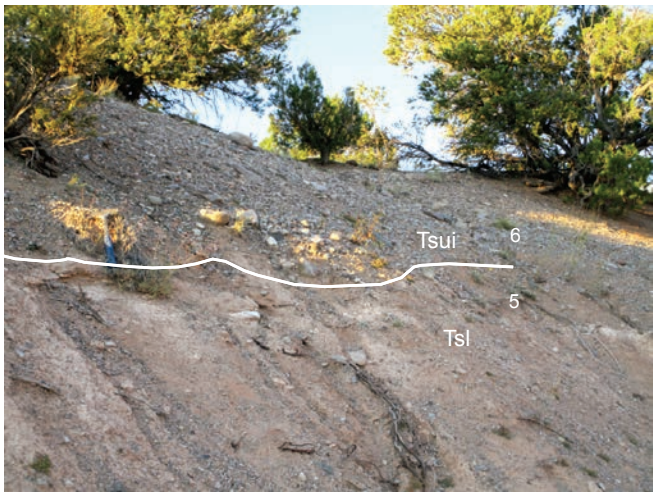

B

C

Figure 10. Photographs of the Sandlin unit at the north and middle Cerro Azul stratigraphic sections. A) View of the middle Cerro Azul stratigraphic section, looking northwards. Numbers refer to stratigraphic section units (see Fig. 7, App. 3). Various lithologic subunits are shown in white text: Tto = Ojo Caliente Sandstone Member of the Tesuque Formation, Tcv = Vallito Member of the Chamita Formation, Tsl = lower Sandlin subunit, Tsui = inset basal gravel of the upper Sandlin subunit, Tsu = upper Sandlin unit. B) Scoured contact at the base of the inset basal gravel of the upper Sandlin unit (Tsui) overlying the lower Sandlin subunit (Tsl). Note the abundance of cobbles in Tsui (strat section unit 6). C) Cemented sandy pebble-conglomerate of strat section unit 4 in the north Cerro Azul stratigraphic section, which has abundant cross-stratification. Average paleoflow from 23 imbricated clasts is 207°. Clast count site A-68 is located ~10 m north of here (Table 2). More Sandlin unit photographs are shown in Appendix 3.

to reddish yellow; sand size is mostly fine- to very coarse-grained and gravels are predominantly very fine to very coarse pebbles. Gravel is coarser (pebbles with 10–15% cobbles and 1% boulders) and clast-supported in the basal sandy gravel underlying the lower Cerro Azul basalt flow (clast count sites J46f and A-52, Figs. 2, 8). In the upper Sandlin subunit, sand is mostly brownish with local areas of reddish yellow; sand size is mostly medium- to very coarse-grained, and gravel contains pebbles and cobbles whose composition is discussed below. Basaltic boulders were locally observed at the base of the upper Sandlin subunit—both in the U.S. Highway 285 paleovalley and to the south of this paleovalley (Fig. 4, Appendix 4). In both the upper and lower Sandlin subunits, gravel is subrounded to subangular and poorly sorted. Overall, the Sandlin unit is weakly consolidated, but moderate to strong cementation by calcium carbonate is locally observed, particularly southeast of Cerro Azul in the lower Sandlin subunit. Sand composition, visually estimated with a hand lens, suggests grains are predominantly quartz with subordinate feldspar and 10–20% lithic grains.

Gravel Composition

The variation of gravel composition within the Sandlin unit gives key information regarding paleogeography and possible source areas (Table 2, Appendix 5). The basal gravel of the lower Sandlin subunit, underlying the lower Cerro Azul flow (Tslbg in Table 2), contains a high proportion of quartzite (49–61%) with subordinate felsic-dominated volcanic rocks (13–19%) and relatively high amounts of Pilar Phyllite (6–16%). Minor amounts of Paleozoic sedimentary rocks (1–10%) and the quartz-porphyry marker clast (up to 5%) were observed. A diverse gravel composition, containing 1–25% Paleozoic clasts and 3–6% of the quartz-porphyry marker clasts, is present in the lower Sandlin subunit above the lower Cerro Azul flow (Tsl in Table 2; Fig. 5). This unit contains less quartzite (13–38%) and less Pilar Phyllite (0–3%) than the subunit's basal gravel, and gabbroic rocks and intermediate intrusives (0–5%) are locally observed.

Two gravel-based petrofacies are differentiated in the upper Sandlin subunit according to percentages of Paleozoic sedimentary clasts, although other gravel types vary as well. These are called the northern and southern petrofacies, based on their relative positions in the studied escarpment. The northern petrofacies (Tsun in Table 2) generally lacks Paleozoic sedimentary clasts (<1%) and has no clasts of Pilar Phyllite. Clast composition is dominated by rhyolite and felsic tuffs (including 1–5% of the Amalia Tuff), with minor granite, intermediate intrusive rocks (commonly greenish due to propylitic alteration), quartzite, dacite, and basalt (Table 2). Included in the felsic volcanic rocks is the quartz-porphyry marker clast (trace to 5% of total gravel; Appendix 4). Also observed in the gravel fraction is 0–1% amounts of gabbro-diorite (Table 2; Appendix 4) and 1–10% basalt. In contrast to the northern petrofacies, the southern petrofacies of the upper Sandlin subunit contains notable amounts of Paleozoic sedimentary clasts (approximately 10–50%; Table 2).

TABLE 2. Clast count data from Pliocene sedimentary deposits in study area

Site: Unit*:	J1 Tsun	J78B Tsus	J19 Tsun	J72 Tsus	J16J Tsus	J82 Tsus	J84 Tsus	J44D Tsus	GTM-756 Tsui	A-68 Tsl	GTM-752a Tsl	GTM-752b Tsui	A-58 Tsl	J46f Tslbg	A-52 Tslbg	A-54 Tsl	TJ-7 Tsui
Quartzite	14%	8%	8%	15%	13%	25%	22%	25%	9%	17%	13%	14%	19%	61%	49%	38%	21%
Tertiary intermediate volcanic	9%	4%	15%	6%	9%	4%	7%	2%	6%	6%	12%	4%	8%	3%	7%	6%	16%
Tertiary felsic volcanic	38%	8%	65%	19%	28%	15%	16%	33%	53%	17%	29%	59%	19%	13%	15%	28%	45%
Paleozic sedimentary	0%	49%	0%	44%	21%	23%	28%	11%	3%	20%	20%	1%	8%	1%	10%	4%	0%
Vein quartz	7%	2%	4%	2%	4%	4%	3%	0%	4%	7%	3%	4%	4%	0%	0%	10%	7%
Proterozoic amphibolite	5%	0%	0%	1%	2%	5%	5%	2%	1%	1%	2%	0%	0%	0%	0%	0%	0%
Pilar Phyllite	0%	0%	0%	0%	trace	0%	1%	0%	0%	0%	3%	0%	0%	16%	6%	1%	1%
Granitic	14%	24%	5%	14%	24%	22%	16%	25%	9%	12%	10%	6%	21%	5%	2%	5%	4%
Servilleta Basalt	8%	5%	2%	0%	0%	0%	0%	1%	11%	0%	8%	12%	0%	0%	0%	5%	5%
Proterozoic schist	3%	0%	2%	0%	0%	0%	0%	0%	0%	6%	0%	0%	11%	0%	5%	0%	0%
Epidote	2%	0%	0%	1%	0%	2%	2%	1%	2%	0%	2%	0%	0%	1%	0%	0%	0%
Gabbro-intermediate intrusives	0%	0%	0%	0%	0%	1%	0%	0%	1%	5%	trace	0%	4%	0%	0%	0%	1%
Other	1%	0%	0%	0%	0%	0%	0%	0%	1%	4%	0%	0%	2%	0%	2%	1%	0%
Quartz-porphyry**										5%			6%		4%	3%	trace
Comments:	Other = carbon-ate nodules	Basal 1-2 m: 2 Pz slst, 1 lm		6 Pz sltst	well-rnded pea gravel		1 Pz 1m	1 Pz lm 2 Pz sltst	Other = uniden-tified		21 Pz ss, 3 Pz sltst	Site is 1.7-1.8m above base		sillimanite in quartz-ite?			
Easting***	419560	419390	419924	419716	419867	419853	419954	419633	419367	419347	419281	419295	418842	418462	418285	418375	417913
Northing***	4022316	4022042	4020992	4020032	4019893	4018329	4017130	4017007	4015310	4015182	4015125	4015138	4013652	4013407	4013270	4013237	4012972

Notes
* Unit abbreviations: Tslbg - lower basal gravel of lower Sandlin subunit; Tsl = lower Sandlin subunit; Tsui = inset basal gravel of upper Sandlin subunit; Tsun & Tsus: upper Sandlin subunit, northern and southern petrofacies, respectively.
** This clast type was subsumed into "Tertiary felsic volcanics" where shaded.
*** These are UTM coordinates in meters; datum is NAD83 (zone 13).

Other major lithologic types include felsic volcanic rocks, quartzite, and granitoids (ranging from white to a distinctive red).

At the base of the U.S. Highway 285 paleovalley lies a 1–2 m thick bed of sandy pebbles and fine to coarse cobbles (Fig. 4). The clasts include 1–40% (mostly 1–5%) Paleozoic sedimentary clasts, felsic to intermediate volcanic rocks, granite and intermediate intrusives (probably granodiorite or diorite), quartzite, ~1% basalt, and trace to 1% gabbroic rocks (Appendix 4). These compositions are consistent with the southern petrofacies of the upper Sandlin subunit. Subrounded to subangular basaltic boulders are also present in this basal bed, increasing in abundance to the north.

South and east of Cerro Azul, the inset gravel at the base of the upper Sandlin subunit is distinctive in its abundance of felsic volcanic rock types (45–59%), similar to the northern petrofacies of the upper Sandlin subunit (Table 2, Fig. 5), and relatively high proportions of Servilleta Basalt (5–12%). Many of the felsic volcanic rocks are aphanitic and flow-banded while some are reddish brown and crystal-rich; both resemble felsic clasts in the Cordito Member of the Los Pinos Formation. Sparse (trace-1%) of the quartz-porphyry marker clast and gabbroic rocks are present. The amount of Paleozoic sedimentary clasts typically is ≤3%, but at one locality they are as high as 10% (i.e., Fig. 9A). One of the most noteworthy features of the inset gravel is cobbles and boulders of Servilleta Basalt that contain approximately 1% phenocrysts of conspicuous olivine, lithologically similar to the upper Cerro Azul basalt flow (Fig. 9).

Pebble composition in a small outcrop at the base of an inferred small paleovalley, located 5 km NNE of Cerro Azul, is similar to the inset basal gravel of the upper Sandlin unit (site GTM-5 in Fig. 3). These pebbles are composed of felsic-dominated volcanic rocks with ~5% quartzite, based on visual estimation. Stratigraphically higher strata 180 m WNW (site J19, Table 2) differ slightly in that they contain 5% granitic clasts.

Paleoflow data

Collectively, paleoflow direction generally ranges from southwest to west for the Sandlin unit (Figs. 2–3, 11; Appendix 6). Clast imbrication taken at a single site in

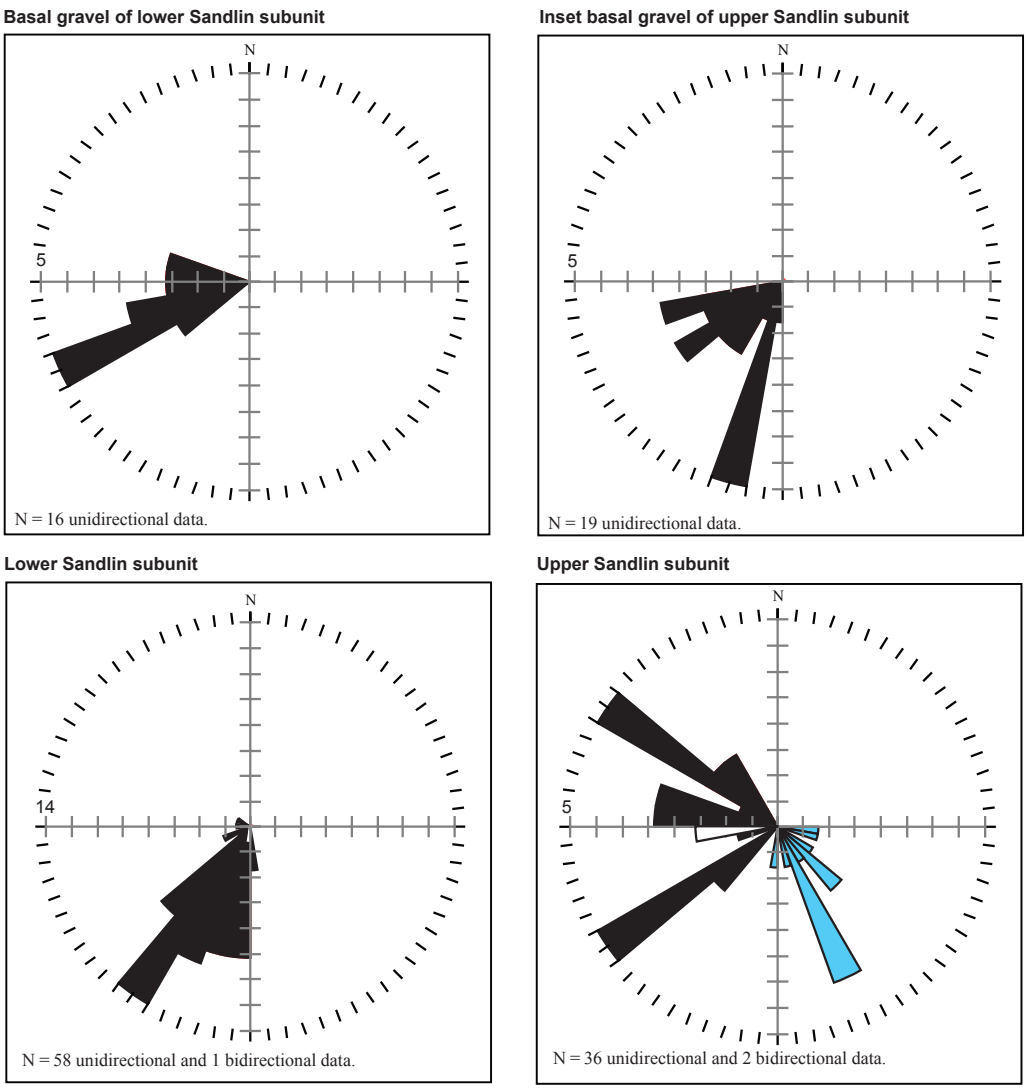

Figure 11. Paleocurrent data for the Sandlin unit plotted on rose diagrams. Black shade indicates unidirectional data from clast imbrication, and the white shade indicates the preferred trend of bidirectional data from channel margins and channel trends. Light blue shade is clast imbrication measurements from site GTM-5, which is interpreted to have been deposited in an older, southeast-trending paleovalley. Bin size is 10° and estimated error is ±15°. Scale of axes (i.e., number of measured clasts per bin) is indicated on left side of each rose diagram.

the basal gravel of the lower Sandlin subunit, beneath the lower Cerro Azul flow, is southwesterly (Fig. 11) with a mean azimuth of 252°. The lower Sandlin subunit above the lower Cerro Azul flow exhibits slightly more southerly paleoflow (means of 207–218°) compared to the basal gravel. The inset basal gravel of the upper Sandlin subunit also has southwesterly paleoflow (mean azimuth of 220°) based on a single locale (subunit 6 of the middle Cerro Azul stratigraphic section, Appendices 3 and 6). At the aforementioned GTM-5 site (Fig. 3), paleoflow was to the southeast (Fig. 11). Otherwise, paleoflow indicators in the upper Sandlin subunit trend northwest to southwest, including clast imbrications in the middle to upper parts of the U.S. Highway 285 paleovalley (Figs. 3, 11).

Volcanic rock descriptions

Basalt flows

Three dated basalt flows provide age control for the Sandlin unit. To the north, the south Comanche Rim basalt flow is 3–6 m thick and appears to be a single flow. This basalt consists of aligned plagioclase laths ≤1.0-mm long, has trace to 0.5% olivine phenocrysts approximately 0.5 mm in diameter, and exhibits inter-crystal voids.

To the south, the upper and lower Cerro Azul flows are both medium- to dark-gray, variably vesicular (0–25% vesicles 0.1–2.0 cm in length), and composed primarily of plagioclase laths ≤1.0-mm long with many inter-crystal voids. Both flows exhibit internal variability but can be distinguished using stratigraphic position (see above), overall size and percentage of olivine phenocrysts, and unit thickness. Overall, the upper Cerro Azul flow has more olivine phenocrysts that tend to be slightly larger (approximately 1–2%, 0.2–2.0 mm long) than seen in the lower Cerro Azul flow (≤0.5% olivine phenocrysts <1.0 mm long). Olivine is locally altered to iddingsite in the upper part of the upper Cerro Azul flow. The lower Cerro Azul flow has trace to 0.5% phenocrysts of pyroxene, which may form reaction rims around olivine, and both olivine and pyroxene are altered to iddingsite. The lower flow is 2.0–2.5 m thick, whereas the upper flow is 5 m thick.

Mesa Vibora

The 120-m tall Mesa Vibora lies 8 km northwest of Cerro Azul and 8 km east of the town of Ojo Caliente (Fig. 1). As mapped and described by Koning et al. (2007a), this topographic feature is capped by 40–45 m of very dark gray to black, non-vesicular basalt whose basal part is intercalated with basaltic tephra and agglutinate (Fig. 12). This basalt is subhorizontal but overlies sand and gravel beds that dip steeply (21–54°) in a radial manner towards the center of the mesa. The sand and gravel becomes more volcaniclastic up-section, allowing subdivision into two units. The upper unit is 150–220 m thick (stratigraphic thickness) and contains pebbles and coarse sand composed primarily, but not exclusively, of basaltic scoria and altered basaltic lapilli cinders; minor basaltic cobbles and boulders are also present. The lower unit (>90–100 m stratigraphic thickness), whose strata also dips steeply inward in a radial manner, consist of non-volcanic, very pale brown to light yellowish brown sand with scattered very fine to very coarse pebbles. The fine- to medium-grained sand fraction is subrounded and similar in composition and texture to the Ojo Caliente Sandstone Member of the

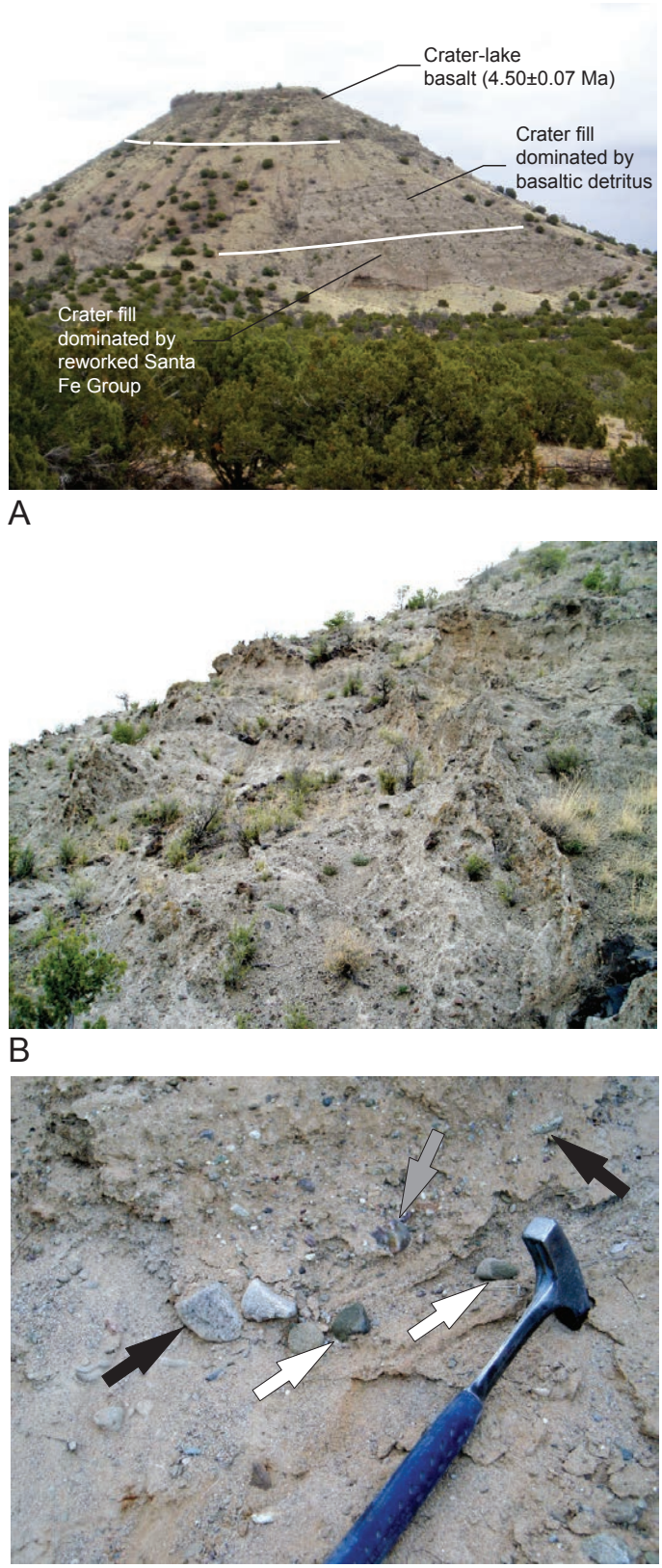

Figure 12. Photographs of Mesa Vibora. A) Northward view of this 120-m (400-ft) tall topographic feature that is interpreted to be an eroded volcanic crater (probably a maar). The upper white line separates shallow crater-fill (diatreme) deposits from the overlying crater-lake basalt. B) Variably cemented, light gray gravelly sand composing the upper part of the shallow crater-fill deposits, as exposed on the south slopes of Mesa Vibora. C) Close-up view of Santa Fe Group sediment reworked into the lower exposed part of the volcanic crater. Larger clasts include greenish Paleozoic sandstones (white arrows), granites and intermediate intrusives (black arrows), and quartzites (gray arrow). Rock hammer for scale.

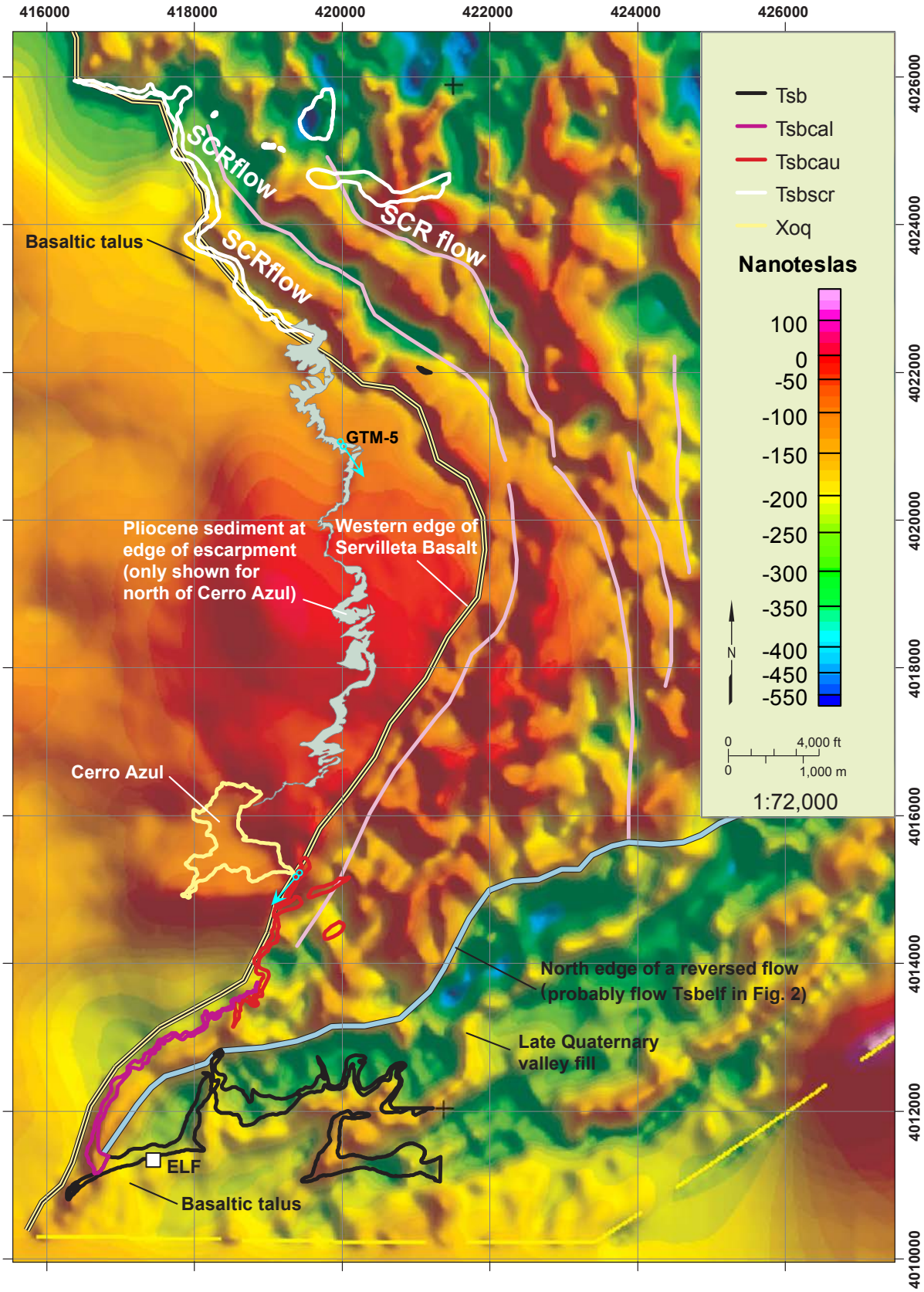

Figure 13. Shaded-relief image depicting reduced-to-pole aeromagnetic data of Bankey et al. (2007), illuminated from the northeast. Map projection is UTM zone 13 using NAD83 datum. The dashed yellow line on the south end of figure demarcates the limit of high-resolution coverage of aeromagnetic data. The labeled, light blue-shaded region illustrates exposed Pliocene sediment at the edge of the escarpment (i.e., upper Sandlin subunit) and the thick yellow line denotes the western edge of Servilleta Basalt, which is buried east of the light blue shade. Pink lines are drawn along the axes of possible paleovalleys. Blue arrows denote paleoflow directions, determined from clast imbrications, for sediment interpreted to relate to these paleovalleys; the lower paleoflow site corresponds to unit 6 of the middle Cerro Azul stratigraphic section. Abbreviations include: SCR flow=south Comanche Rim flow; ELF=Embudo local fauna site; Tsb=undifferentiated Servilleta Basalt. Other abbreviations follow those of Figure 2.

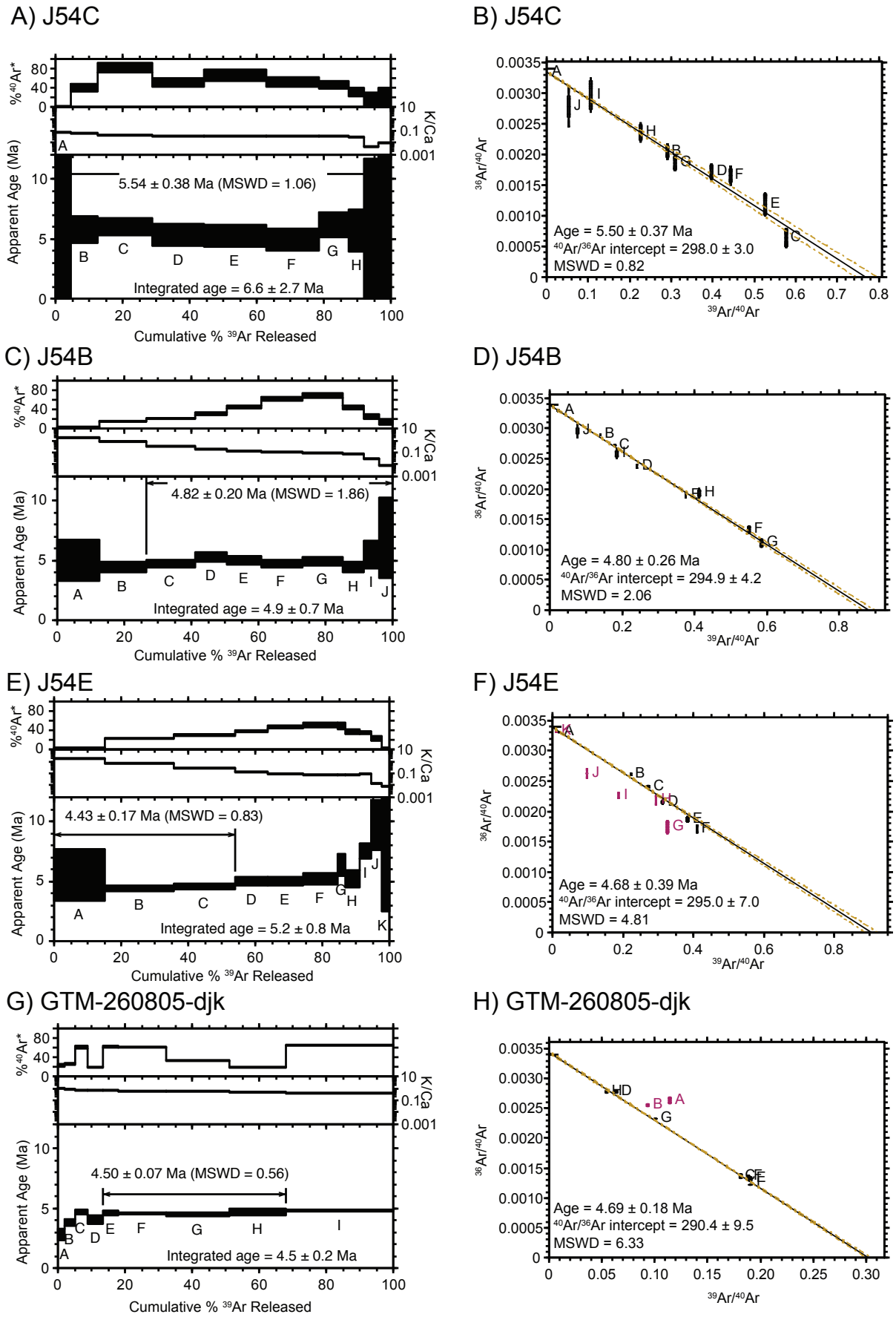

Figure 14. Age spectra and inverse isochron plots for dated basalt samples. Data points in purple on the inverse isochron were not included in the age calculation. Data shown with 1σ errors and weighted mean reported at 2σ error. Sample locations and interpreted ages are given on Table 3.

TABLE 3. Summary of new and previously published $^{40}Ar/^{39}Ar$ ages for basalts near Cerro Azul

Sample	Location in UTM coordinates, in meters (zone 13, NAD 83)	Map unit (informal names)	Lab sample number	Heating steps	Age ± 2σ (Ma)	MSWD*	Comments
J54B	418,918 E 4,013,776 N	Upper Cerro Azul basalt flow (Tsbcau)	57452	8	4.82 ± 0.20	1.86	
J54C	418,462 E 4,013,407	Lower Cerro Azul basalt flow (Tsbcal)	57457	9	5.54 ± 0.38	1.06	
J54E	419,940 E 4,022,545 N	South Comanche Rim basalt flow (Tsbcr)	57455	3	4.43 ± 0.17	0.83	
RA-080	419,940 E 4,022,545 N	South Comanche Rim basalt flow (Tsbcr)	6992	12	4.69 ± 0.09	2.28	From Appelt (1998); Inverse isochron
GTM-260805-djk	410,930 E 4,019,404 N	Capping basalt on Mesa Vibora, interpreted to have been a crater lake	57183	6	4.50 ± 0.07	0.56	
RA-055	410,909 E 4,018,809 N	Capping basalt on Mesa Vibora, interpreted to have been a crater lake	6119	4	4.55 ± 0.12	1.67	From Appelt (1998)

Notes: Analyses performed at the New Mexico Geochronology Research Laboratory. Ages calculated relative to FC-2 Fish Canyon Tuff sanidine interlaboratory standard (28.201 Ma, Kuiper et al., 2008). Samples J54B, J54C, J54E, RA-080, and RA-055 were step-heated using a Mo double-vacuum resistance furnace, whereas sample GTM260805-djk was step-heated using a defocused CO^2 laser. Groundmass dated in all samples.
* MSWD = Mean square weighted deviation.

Tesuque Formation. We interpret these clastic deposits as a shallow crater-fill diatreme facies associated with a likely maar (now eroded), which is capped by a basalt that solidified as a crater-filling lava lake. Mesa Vibora is useful for reconstructing the paleogeographic location of our studied fluvial system because its exposed shallow-facies diatreme fill, particularly the lower unit, contains large, subrounded clasts that compositionally match the southern petrofacies of the upper Sandlin subunit: greenish Paleozoic sandstone, rhyolite, dacite, granite and intermediate intrusives (granodiorite?), the quartz-porphyry marker clast, and trace gabbro-diorite, listed from most to least abundant (Fig. 12).

Aeromagnetic Data Interpretation

We utilized reduced-to-pole aeromagnetic data to interpret earliest Pliocene, basalt-filled paleovalleys as well as to refine the age of the south Comanche Rim basalt. Textural differences in the shaded relief image of the data demarcate the western limit of basalts buried by the Sandlin unit (thick yellow line, Fig. 13). Terrain underlain by shallowly buried (<300 m) Servilleta Basalt produces sharply mottled textures due to varying intensities of remanence in basaltic lavas (Fig. 13); similar aeromagnetic textures are commonly observed in other Rio Grande Pliocene basalts (Grauch et al., 2004, 2006).

A conspicuous feature of the aeromagnetic imagery are troughs and ridges, the former being annotated by pink lines on Figure 13. These features trend northwest-southeast in the northern half of Figure 13, parallel to the buried edge of the basalt flows, and either northeast-southwest or north-south in the southern part of Figure 13. The steep magnetic gradients alongside these features are produced by the juxtaposition of materials possessing different magnetic properties. The most reasonable causes of this juxtaposition are faulting or buttress contact relations (Grauch and Hudson, 2007). We favor the interpretation of buttress relations along margins of narrow (about 500-800 m wide) paleovalleys because 1) basalts do not appear to be faulted along the Comanche Rim; 2) the curvilinear aeromagnetic trends are similar to the fluvial paleocurrent trends in two inferred, small paleovalleys (i.e., site GTM-5 and the inset base of the upper Sandlin subunit in the middle Cerro Azul stratigraphic section); and 3) the trends of the magnetic gradients are oblique to the NE-SW striking Embudo fault system to the south, which represents the dominant fault system active in the region since the Pliocene (Muehlberger, 1979; Kelson et al., 2004; Koning et al., 2004a).

To varying degrees, we can interpret Servilleta basaltic lavas with normal-polarity remanence versus those with reversed-polarity remanence. This is particularly important for constraining the age of the southern Comanche Rim flow. We interpret reversed-polarity remanence for this flow because it commonly corresponds to aeromagnetic lows at the top of topographic escarpments (Fig. 13).

Radioisotopic age control

$^{40}Ar/^{39}Ar$ age spectra and inverse isochron plots for basalt samples are shown in Figure 14. A summary of stratigraphically relevant basalt ages, from both this study and a previous investigation (Appelt, 1998), is reported in Table 3. Basaltic groundmass was dated in all the samples. Plateau ages are the preferred eruption ages because the samples do not contain excess ^{40}Ar (i.e., the $^{40}Ar/^{36}Ar$ intercept is within error of the atmospheric value of 295.5; Nier, 1950). A plateau is defined using two criteria: 1) three or more contiguous steps comprising more than 50% of the ^{39}Ar released in the age spectrum, and 2) the ages of steps overlap at 2σ error (Fleck et al., 1977). We discuss ages, reported at 2σ error, from oldest to youngest.

The lower and upper Cerro Azul flows yielded

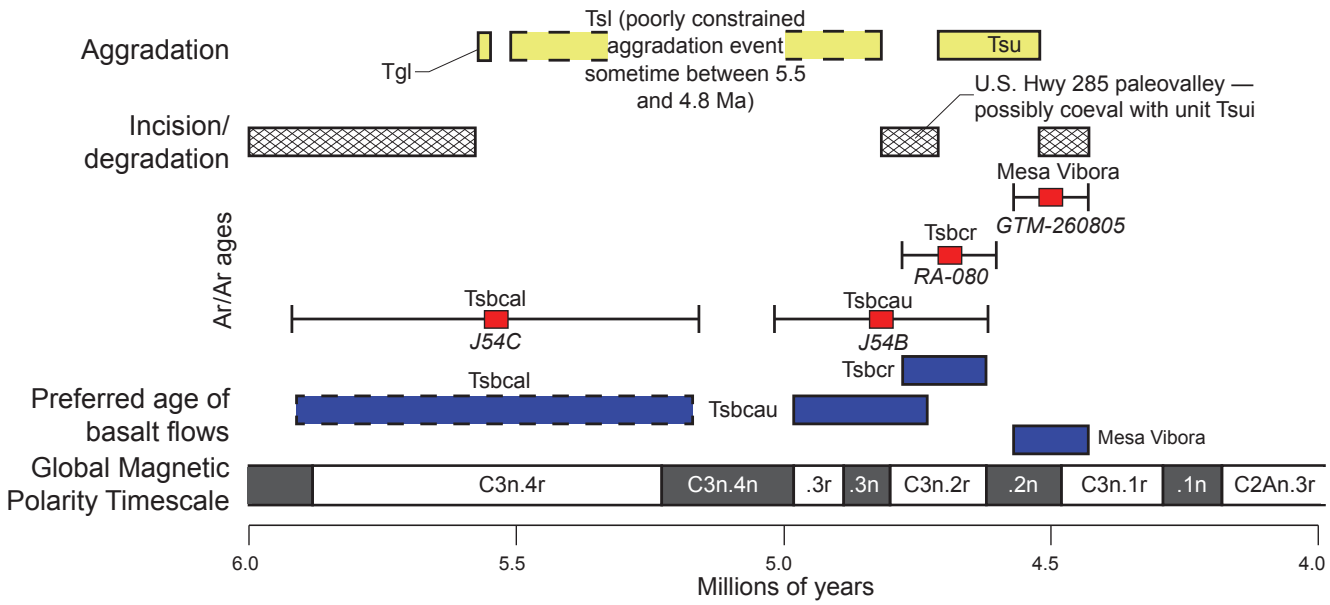

Figure 15. Illustration of our preferred basalt ages (brackets indicate 2σ errors) and timing of aggradation and incision events in the study area. Also shown is the geomagnetic polarity timescale (Ogg, 2012) and basalt $^{40}Ar/^{39}Ar$ ages with their 2-sigma errors (Fig. 14, Table 3).

statistically distinguishable ages. The lower Cerro Azul flow (sample J54C, Fig. 14A) returned a plateau age of 5.54±0.38 Ma and the corresponding inverse isochron indicates a $^{40}Ar/^{36}Ar$ intercept of 298.0±3.0 (Fig. 14B). The upper Cerro Azul flow (sample J54B, Fig. 14B) yielded a plateau age of 4.82±0.20 Ma and also does not contain excess ^{40}Ar (Fig. 14D). The plateau ages for the upper and lower Cerro Azul flow, combined with the stratigraphic relations described above (Fig. 7), indicate that the lower Sandlin unit in the southern part of the study area was deposited within the 0.72±0.58 Ma interval between the emplacement of these lavas.

The south Comanche Rim basalt at U.S. Highway 285 (Fig. 3) was dated by both this study (sample J54E) and by Appelt (1998, sample RA-080). Sample J54E yielded a plateau age of 4.43±0.17 Ma (Fig. 14E). Excluding the high-temperature steps, the inverse isochron indicates an atmospheric argon-trapped component (Fig. 14F). Sample RA-080 contains excess ^{40}Ar ($^{40}Ar/^{36}Ar$ intercept = 299.1±1.2), yielding an inverse isochron age 4.69±0.09 Ma (age recalculated relative to FC- 2 equal to 28.201 Ma; original data reproduced in Appendix 7 of this manuscript). Although these two ages are statistically indistinguishable at 2σ, the preferred eruption age for the south Comanche Rim basalt is the inverse isochron age of RA-080 for three reasons. First, the spectrum for J54E displays a rising release pattern possibly related to ^{40}Ar loss. Accordingly, the plateau age of J54E should be considered a minimum age estimate. Second, the inverse isochron age of RA-080 is more precise than J54E. Third, the 4.69±0.09 Ma age is consistent with aeromagnetic data suggesting the flow was erupted during a reversed magnetic polarity chron (Fig. 15).

Basalt groundmass from the crystallized crater lake capping Mesa Vibora yielded a plateau age of 4.50±0.07 Ma (GTM-260805-djk, Fig. 14G). The inverse isochron yielded a $^{40}Ar/^{36}Ar$ intercept of 290.4±9.5 Ma, within error of atmospheric values (Fig. 14H). One of two previously published ages (Appelt, 1998) from the solidified crater lake is 4.55±0.12 Ma (age recalculated relative to FC-2 equal to 28.201 Ma; original data reproduced in Appendix 7) and is analytically indistinguishable from our plateau age. Thus, we interpret the plateau age of 4.50± 0.07 Ma to accurately represent the eruption age of Mesa Vibora.

Discussion

Sandlin unit

Provenance

Provenance interpretations of the Sandlin unit are based on paleoflow data and the presence of unique gravel types in its subunits (i.e., northern and southern petrofacies of the upper Sandlin subunit; lower Sandlin subunit and its basal gravel underlying the lower Cerro Azul basalt flow). Data indicate paleoflow was primarily towards the west or southwest, with one site (GTM-5) indicating southeast paleoflow (Fig. 11). Therefore, the primary source areas are interpreted to lie primarily east and northeast of the study area, with a secondary source to the north. Potential source areas correspond to the Picuris Mountains, the southern Taos Mountains east and southeast of Taos, the central Taos Mountains northeast of Taos, and the border area between the eastern Tusas Mountains and Taos Plateau (Fig. 1).

We interpret the southern petrofacies of the upper Sandlin subunit, as well as the lower Sandlin subunit, to have been derived, in part, from the southern Taos Mountains. The southern petrofacies of the upper Sandlin unit contains Paleozoic sedimentary clasts (10–50%, Table 2, Fig. 5). The local presence of gabbroic clasts (site J82, Table 2) suggests some contribution from the central Taos Mountains. Likewise, the presence of local Pilar Phyllite (site J84, Table 2) suggests partial contribution from the Picuris Mountains. The remainder of the gravel types in the southern petrofacies could have been derived from either the Picuris Mountains or the central Taos

Mountains. For example, the felsic-dominated volcanic gravels could be recycled from the Picuris formation (as defined by Rehder, 1986, and Aby et al., 2004) in the eastern Picuris Mountains, Chama-El Rito Member (Tesuque Formation) at the northern base of the Picuris Mountains, the Los Pinos Formation along the eastern flanks of the Tusas Mountains, or directly transported from the Latir volcanic field (Fig. 1). With some exceptions, the clast compositions of the lower Sandlin subunit are similar to the southern petrofacies of the upper Sandlin subunit. Notable differences include less Paleozoic clasts and overall more Pilar Phyllite in the lower Sandlin subunit (Table 2).

The northern petrofacies of the upper Sandlin subunit is interpreted to be derived from the central Taos Mountains, consistent with its northerly position and westerly paleoflow indicators. This petrofacies lacks Paleozoic sedimentary clasts and Pilar Phyllite, so its provenance is not in the southern Taos Mountains or the Picuris Mountains. Gabbroic and intermediate intrusive rocks, some of the latter being propylitically altered, as well as observations of the quartz-porphyry marker clast (Appendix 4), are best matched with the central Taos Mountains. The copious volcanic rocks in the northern petrofacies were derived from the Latir volcanic field or reworked from the Los Pinos Formation.

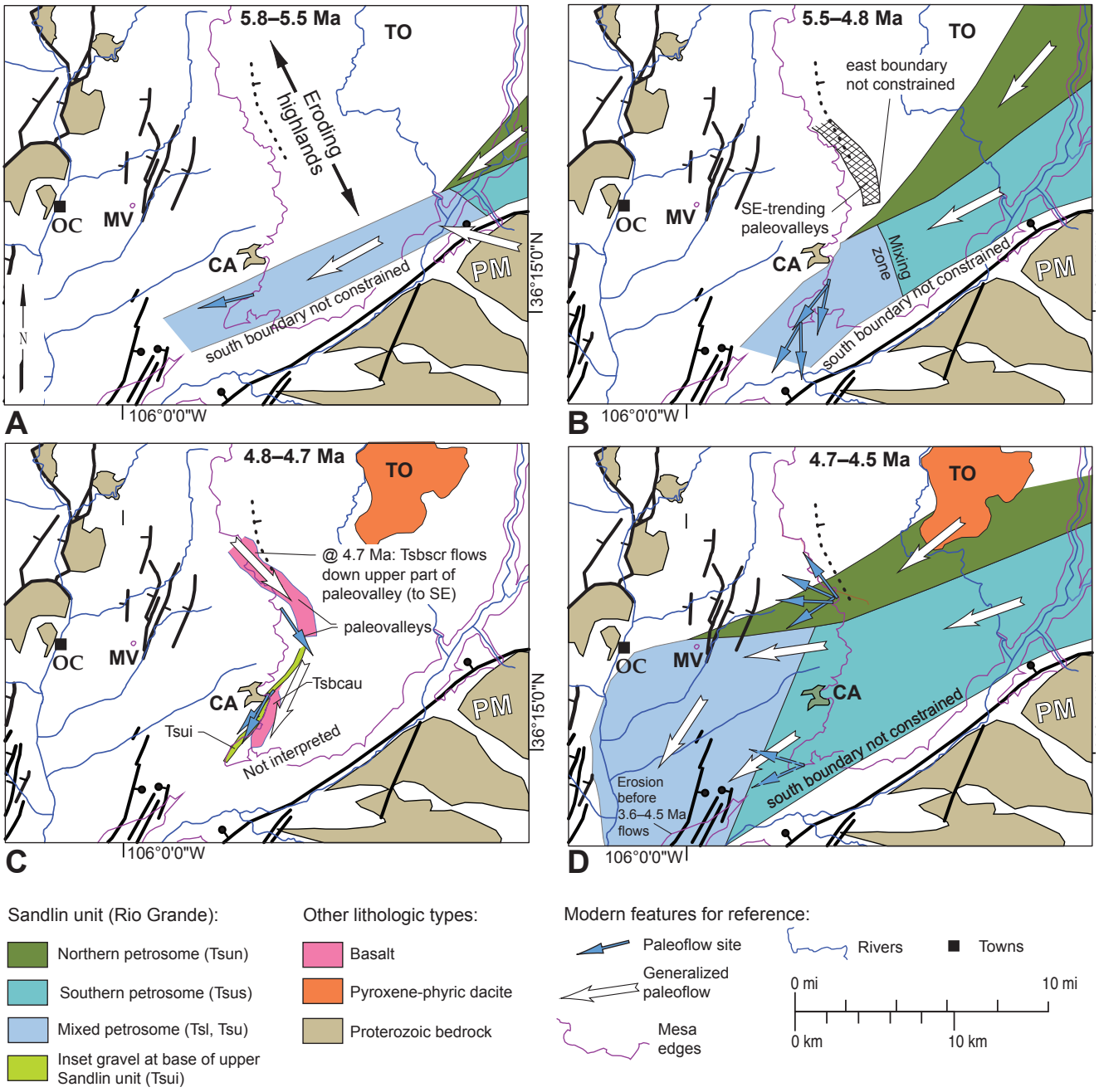

Figure 16. Paleogeographic maps illustrating the following sequence of events: A) general erosion prior to the 5.54±0.38 Ma basalt; B) Aggradation of lower Sandlin unit sometime between emplacement of the 5.54±0.38 Ma and 4.82±0.20 Ma basalts, concomitant with probable southeast-trending paleovalley development to the north; C) Emplacement of the informal upper Cerro Azul flow (Tsbcau, 4.82±0.20 Ma) and development of a paleovalley along its northwestern flank, which was later back-filled by unit Tsui; to the north, the informal south Comanche Rim basalt (Tsbscr) flowed down a southeast-trending paleovalley at 4.69±0.09 Ma; and D) General aggradation between emplacement of the 4.69±0.09 Ma south Comanche Rim flow and the 4.50 ± 0.07 Ma Mesa Vibora basalt; not shown is 5-6 m of incision of the U.S. Highway 285 paleovalley immediately(?) after emplacement of the south Comanche Rim flow. Blue lines are modern drainages for reference. Abbreviations of modern-day features: CA = Cerro Azul, MV = Mesa Vibora, OC = Ojo Caliente, PM = Picuris Mountains, TO = Tres Orejas.

The basal gravel of the lower Sandlin subunit, underlying the lower Cerro Azul basalt, differs from higher strata in the lower Sandlin subunit. The high abundance of quartzite and Pilar Phyllite indicates a significant contribution from the northern Picuris Mountains. However, the presence of the quartz-porphyry marker clast and 1–10% Paleozoic clasts (Table 2) indicates that the river depositing this gravel also drained the southern and central (and possibly northern) Taos Mountains.

The inset base of the upper Sandlin subunit has a very high proportion of volcanic clasts (~60%) that include 5–12% basaltic gravel interpreted as reworked Servilleta Basalt. Lacking clasts of Pilar Phyllite, it is relatively similar to the northern petrofacies and interpreted to be derived from the north or northeast. This gravel does have minor amounts of Paleozoic sedimentary clasts (typically ≤3%), which are possibly reworked from the lower Sandlin subunit.

Similar volcanic-dominated gravel is observed 5 km NNE of Cerro Azul at site GTM-5 (Fig. 3). Paleoflow there was clearly toward the southeast (Fig. 11). We interpret that this relatively fine gravel to have possibly filled a small, southeast-trending paleovalley that drained volcaniclastic sedimentary terranes of the Cordito Member (Los Pinos Formation) in the Tusas Mountains–Taos Plateau border region.

From our clast-count and paleocurrent data, we interpret two rivers sourced in the central Taos Mountains and southern Taos Mountains–Picuris Mountains to have flowed and merged west-southwestward (Figs. 2, 3, 11, 16). The associated drainage basins, if similar to those of the modern Rio Pueblo de Taos and the Rio Grande–Red River system north of Rio Pueblo de Taos, would have each been >500 km^2. The northern and southern petrofacies of the upper Sandlin subunit are interpreted to be associated with the northern and southern of these two rivers, respectively. Lower Sandlin gravel is more mixed than that of the upper subunit, with a major contribution from the Picuris Mountains in its lower basal gravel (Fig. 5). This implies that during deposition of the lower Sandlin subunit the two rivers effectively merged upstream of the study area (Fig. 16).

Ancestral Rio Grande drainage characteristics at 5.5–4.5 Ma

We interpret the Sandlin unit to have been deposited by two merging, bedload-dominated rivers exiting the southern San Luis Basin. Sediment is relatively poorly sorted, channel-fills are typically stacked, and bar-related cross-stratification is common; clay-silt overbank deposits are lacking. The absence of reduced mudstones and local presence of massive sedimentary intervals (suggesting periods of bioturbation) suggest the two rivers were largely ephemeral. When the fluvial system was confined in paleovalleys, such as the southern paleovalley filled by the 5.54±0.38 Ma lower Cerro Azul basalt or the U.S. Highway 285 paleovalley filled by the 4.69±0.09 Ma south Comanche Rim basalt, there was sufficient competency to transport higher amounts of cobbles and boulders. However, during major aggradational phases the discharge was spread out over a wider area via flow in multiple channels, each likely tens of meters in width. This dispersed flow resulted in reduced shear stresses because of reduced flow depths and a corresponding decrease in stream competency. We favor deposition by relatively wide and shallow, braided, ephemeral river(s) rather than distal alluvial fans because of: 1) sedimentary characteristics consistent with such a river, and 2) evidence of gravel mixing from the two provenances (particularly in the lower Sandlin unit), which one would not expect in an alluvial fan. We cannot rule out two converging, braided rivers on distal-most reaches of coalescing alluvial fans, although such fans would be uncharacteristically elongated (width to length ratios of 0.3–0.5).

The two merging tributaries of the ancestral upper Rio Grande flowed west-southwest before turning southwesterly and flowing near the present western margin of Black Mesa (Fig. 16), consistent with paleocurrent directions at the latter (Koning and Manley, 2003; Koning, 2004). Prior to 4.50±0.07 Ma, the ancestral Rio Grande flowed as far north and west as Mesa Vibora, which contains gravels similar to the southern petrofacies of the upper Sandlin subunit with provenance in the central and southern Taos Mountains (Fig. 16). The coarseness of the gravel (coarse to very coarse pebble sizes, Fig. 12) effectively excludes it from being part of the Vallito Member of the Chamita Formation.

Paleo-geographic and paleo-drainage evolution

We interpret the following series of events across the Mio-Pliocene boundary for the fluvial system exiting the southern San Luis Basin (Fig. 16). Previously (sometime in the late Miocene), the Vallito Member was deposited by a low competency fluvial system that had similar provenance and drainage characteristics as the Sandlin unit; slow aggradation rates combined with bioturbation produced a relatively massive sedimentary package. Erosion occurred prior to the 5.54±0.38 Ma lower Cerro Azul basalt flow. This erosion thinned or removed the Vallito Member (Chamita Formation) south of Cerro Azul and formed a west-southwest trending paleovalley approximately 4–7 km wide (Figs 4, 16). A high-competency river occupied the floor of this paleovalley and deposited relatively thin, cobbly gravels. After emplacement of the 5.54±0.38 Ma lower Cerro Azul flow, and prior to the emplacement of the 4.82±0.20 Ma upper Cerro Azul basalt, this paleovalley back-filled with 10–12 m of sand and pebbly sand of the lower Sandlin subunit. Available exposures do not exhibit paleosols nor is there evidence of strongly developed calcic soils on poorly exposed slopes, suggesting that the duration of aggradation could have been relatively short.

Emplacement of the 4.82±0.20 Ma upper Cerro Azul basalt flow, which probably flowed southwestward near the northern margin of the aforementioned paleovalley, locally impacted drainages in the study area, as reflected in the inset basal gravel of the upper Sandlin subunit. The presence of large basalt boulders (up to 3 m in diameter) eroded from the upper Cerro Azul flow, locally cemented within this gravel (Fig. 9), indicates that the stream/river depositing the sediment carved a small paleovalley (possibly only 100–200 m wide) alongside the northwestern margin of the flow. As discussed above, the clast composition of the inset gravel is consistent with a northerly provenance (Fig. 16). We interpret this basalt flow to have blocked south-flowing streams associated with the interpreted south-trending paleovalleys in the aeromagnetic data (Fig. 13). These streams coalesced into a single drainage of relatively high stream power and erosive capability, leading

to meter-scale incision and undercutting of the adjoining basalt flow in the study area. The small paleovalley that paralleled the edge of the basalt flow was back-filled by the basalt boulder-bearing, inset basal gravel (Tsui) of the upper Sandlin subunit. Because of the paucity of Picuris Mountain and southern Taos Mountain gravel in this inset gravel, we infer that rivers/streams derived from these sources may have flowed around the southern margin of the upper Cerro Azul flow.

Aggradation of the upper Sandlin subunit continued after emplacement of the 4.82±0.20 Ma upper Cerro Azul flow and likely buried this lava. Sediment was deposited by two merging rivers associated with the two petrofacies of this subunit, and the north-south width of the depositional area was likely ≥10 km. With time, deposits of the northern river prograded southwards over those of the southern river, based on mapping of the subunit's petrofacies (Figs. 2–4). East of Cerro Azul, the inset basal gravel is overlain by 12–20 m of medium- to very coarse-grained sand, pebbles, and minor cobbles of the upper Sandlin subunit. Upper Sandlin subunit aggradation also buried the 4.69±0.09 Ma south Comanche Rim basalt flow, so its deposition likely continued until 4.6–4.5 Ma. Basalt boulders, presumably eroded from the Servilleta Basalt, are found in basal upper Sandlin deposits south of the U.S. Highway 285 paleovalley (e.g., Fig. 4). The presence of these Servilleta Basalt boulders indicate that these topographically high Sandlin deposits are Pliocene in age and post-date the basal gravel of the lower Sandlin unit—as opposed to being a latest Miocene, post-Vallito Member gravel laid down prior to the incision immediately predating the Sandlin unit.

During early aggradation of the upper Sandlin subunit there was a brief(?) episode of incision and drainage reorganization in the U.S. Highway 285 paleovalley following emplacement of the 4.69±0.09 Ma south Comanche Rim basalt. This basalt likely flowed southeast down the set of aforementioned paleovalleys associated with the inset basal gravel (Fig. 13, site GTM-5), but after its emplacement several meters of incision deepened the U.S. Highway 285 paleovalley and eroded this flow—based on mapping of its lower contact and the increased abundance of basaltic boulders and cobbles to the north in the paleovalley's basal strata (Figs. 3–4). Gravel at the base of this inset paleovalley is associated with the southern petrofacies. This composition, and the fact that paleoflow higher in the paleovalley trend was westward, indicate a drainage reorganization from southeast-flowing (during emplacement of the south Comanche Rim basalt) to west-flowing (upper Sandlin unit). Subsequent aggradation deposited as much as 25 m of basalt-bearing sand and gravel that eventually buried the highest paleotopography between Cerro Azul and U.S. Highway 285 (Figs. 3–4 and 16). Given the relatively poor exposure of the Sandlin unit, it is conceivable there could be other incisional events south of the U.S. Highway 285 paleovalley within the overall aggradation interpreted between 4.8–4.5 Ma and between 5.5–4.8 Ma.

After the 4.8–4.5 Ma aggradation, the fluvial system began to incise. We lack age control to date this switch in the study area or at Mesa Vibora. However, stratigraphic relations on the western escarpment of Black Mesa to the south of the study area clearly indicate that degradation occurred before emplacement of the 4.5–3.3 Ma flows

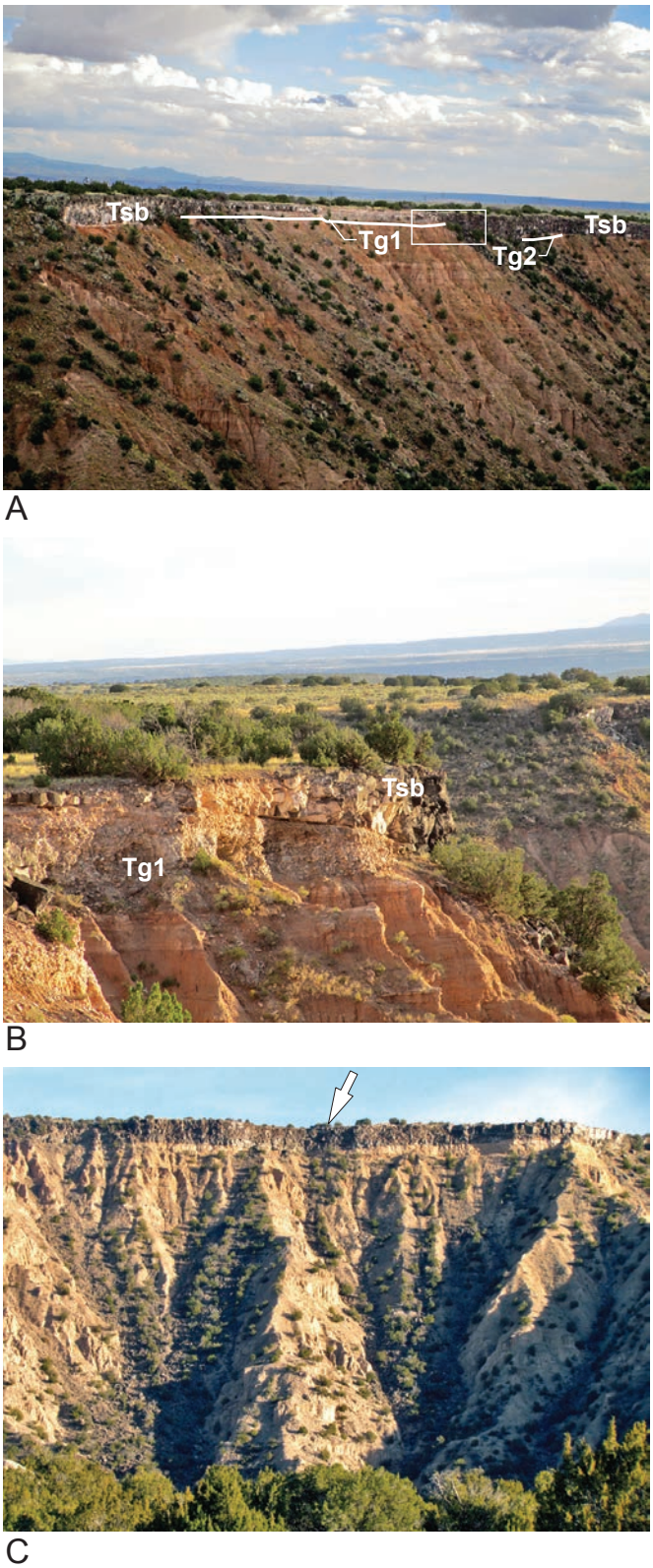

Figure 17. Photographs illustrating erosion on the western side of Black Mesa, east of Vallito Peak, prior to emplacement of 4.5–3.6 Ma Servilleta Basalt (see Fig. 1 for location). A) A cobbly sandy gravel (labeled Tg1) underlying the basalt has been eroded away in many places. Tg2 is a slightly younger gravel underlying the floor of a small paleovalley that is inset into Tg1. Rectangle corresponds to photo in B. Tsb = Servilleta Basalt. B) Note the basalt filling a 5–6 m (approx.) deep paleovalley incised into the Tg1 sandy gravel. C) View of west side of Black Mesa 4 km north of the Rio Chama. Arrow denotes a small, basalt-filled paleovalley that is probably 2–3 m deep.

that cap this mesa (age control from A.W. Laughlin et al., unpubl. in Dethier and Reneau, 1995; Maldonado and Miggins, 2007; Koning et al., 2011; Maldonado et al., 2013; Repasch et al., 2015b). These relations include the formation of small paleovalleys that were later back-filled by the mesa-capping basalts (Fig. 17). This erosion presumably removed most of the upper Sandlin subunit that once extended over the upper Cerro Azul basalt flow (Fig. 4).

Causes of Aggradation

Tectonic or climatic forcings control aggradation via preservation of sediment or adjustments to sediment and water discharges. Determining the relative roles of each is difficult. Although we cannot definitively determine what caused aggradation, we explore possible drivers.

Paleoclimatic conditions may have caused aggradation of the lower and upper Sandlin subunit. Intense precipitation events at this time, coinciding with intensification of the North American monsoon and perhaps coupled with low vegetation density (Chapin, 2008), may have promoted erosion in drainage catchment areas. A relatively high sediment-to-water ratio in the study area's fluvial system may have induced the two aggradational episodes associated with the upper and lower Sandlin subunits.

A postulated tectonic mechanism to trigger the two aggradational events involves reduced slip rates along the Embudo and Sangre de Cristo fault systems. These two faults are directly linked (Kelson et al., 2004), so that reduced lateral slip rates on the Embudo fault should translate to reduced vertical slip rates on the Sangre de Cristo fault. The observation of 4.87±0.30 Ma basalt flowing 0.5 km onto the footwall of the Embudo fault on La Mesita (Koning and Aby, 2003; Koning et al., 2013—age recalculated relative to FC-2 equal to 28.201 Ma) suggests the lack of a tall fault scarp at that time, consistent with low vertical slip rates. A possible way to reduce slip rates is crustal dilation associated with injection of numerous north-south trending dikes at the beginning of major extrusion of Servilleta Basalt (approximately 4.8 Ma), a phenomena interpreted for parts of the East African Rift (Ebinger et al., 2013). Reduced vertical slip rates would lead to less accommodation in the structurally deeper parts of the southern San Luis Basin and less trapping of sediment, thereby promoting westward expansion of Taos Mountain-derived aggradation and a westward migration of the confluence of streams/rivers draining the central and southern Taos Mountains. This is consistent with the general westward migration of the confluence of the northern and southern tributary rivers (Fig. 16).

Implications for Rio Grande evolution

Lowest Pliocene sediment of the Sandlin unit is coarser than the underlying upper Miocene Vallito Member of the Chamita Formation, and this may have implications for the southward expansion of the ancestral Rio Grande from the southern Albuquerque Basin ca. 6–5 Ma. Both the Sandlin unit and the Vallito Member contain similar clast types, consistent with deposition by the same fluvial system of similar provenance. But the maximum clast sizes of the Sandlin unit are typically coarse to very coarse pebbles and cobbles (with local boulders), whereas the maximum clast size in the Vallito Member is only very fine to medium pebbles. Two explanations for this increase in clast size are 1) increased stream power due to enhanced stream discharges (ephemeral or perennial) perhaps related to intensification of the North American monsoon (Chapin, 2008), or 2) decreased eastward tilt rates of the southern San Luis Basin due to lower tectonic subsidence rates, allowing development of steeper westward stream profiles. The tectonic changes of the second explanation may have occurred concomitantly with paleoclimatic changes. Because clast size increases occur prior to the oldest dated basalt flow in the Taos Plateau (i.e., basal gravel of the lower Sandlin subunit beneath the 5.54±0.38 Ma lower Cerro Azul flow), we discount the possibility that stream competency increased due to incision of rivers into newly erupted basalt flows, although this could be a factor in younger Sandlin strata.

If correct, these postulated paleoclimate and tectonic explanations would promote fluvial spillover southward from the Albuquerque Basin ca. 6–5 Ma, given these assumptions: 1) increased discharges and gravel sizes (from the studied paleodrainage and also the Rio Chama) reflect increased sediment flux rate into the Albuquerque Basin; and 2) decreased rates of tectonic subsidence in the southern San Luis Basin typified the northern Rio Grande rift at the Mio-Pliocene transition—resulting in less trapping of sediment compared to earlier in the Miocene. Either explanation would likely have increased sediment delivery into the Albuquerque Basin, completely filling this previously closed basin and allowing fluvial spillover into adjoining basins to the south (Connell et al., 2005, 2012).

Conclusions

The merging tributaries of the ancestral Rio Grande draining the southern San Luis Basin did not steadily incise during the earliest Pliocene into a discrete paleovalley near the modern river. Rather, this fluvial system experienced 10^4–10^5 yr aggradational episodes, punctuated by at least two incisional events, so that by 4.6–4.5 Ma at least 10–25 m of pebbly sand (the Sandlin unit) accumulated as far north as 14 km from the present position of the Rio Grande. Between 4.82±0.20 Ma and 4.50±0.07 Ma, aggradation in the northern part of the study area caused back-filling of previous southeast-trending paleovalleys. Westerly and southwesterly paleocurrent data and gravel-provenance interpretations indicate that the Sandlin unit was deposited by two merging rivers: one sourced in the central Taos Mountains and one sourced in the southern Taos Mountains and northern Picuris Mountains. This fluvial system flowed as far north and west as Mesa Vibora before turning southwestwards down the axis of the Española Basin.

The Sandlin unit is coarser than underlying late Miocene sediment of the Vallito Member (Chamita Formation), but both appear to be derived from similar source areas. Possible reasons for this coarsening across the Mio-Pliocene boundary include climate modulated hydrologic factors (i.e., sediment vs. water discharge ratios) or a reduction of eastward tilt rates of the southern San Luis Basin half graben. Either of these phenomena could have promoted fluvial spillover that occurred through the southern Albuquerque Basin at about this time, allowing a southward expansion of the ancestral Rio Grande into southern New Mexico.

Acknowledgements

This project was supported by the STATEMAP program (National Cooperative Geologic Mapping Program of the U.S. Geological Survey) and the New Mexico Bureau of Geology and Mineral Resources. Lisa Peters and students at the New Mexico Geochronology Research Laboratory helped to prepare separates and generate ages. Karl Karlstrom offered comments in the field. Marisa Repasch reviewed an earlier draft of the mansucript. We thank David Dethier, Steve Cather, and an anonymous reviewer for formal reviews of this paper. Any use of trade, product, or firm names is for descriptive purposes only and does not imply endorsement by the U.S. Government.

References

Aby, S.B., and Morgan, G.S., 2011, The Embudo Local Fauna from a high altitude Pliocene fossil site in Rio Arriba County, New Mexico [minipaper], in Koning, D.J., Karlstrom, K.E., Kelley, S.A., Lueth, V.W., and Aby, S.B., eds., Geology of the Tusas Mountains and Ojo Caliente Area: New Mexico Geological Society, 62nd Annual Field Conference, Guidebook, p. 100–101.

Aby, S.B., Bauer, P.W., and Kelson, K.I., 2004, The Picuris Formation: A late Eocene to Miocene sedimentary sequence in northern New Mexico, in Brister, B.S., Bauer, P.W., Read, A.S., and Lueth, V.W., eds., Geology of the Taos Region: New Mexico Geological Society, 55th Annual Field Conference, Guidebook, p. 335–350.

Aby, S., Karlstrom, K., Koning, D.J., and Kempter, K., 2010, Geologic map of the Las Tablas quadrangle, Lincoln County, New Mexico: New Mexico Bureau of Geology and Mineral Resources Open-File Geologic Map 200, scale 1:24,000.

Appelt, R.M., 1998, $^{40}Ar/^{39}Ar$ geochronology and volcanic evolution of the Taos Plateau volcanic field, northern New Mexico and southern Colorado [M.S. thesis]: Socorro, New Mexico Institute of Mining and Technology, 58 p.

Baldridge, W.S., Damon, P.E., Shafiqullah, M., and Bridwell, R.J., 1980, Evolution of the central Rio Grande rift, New Mexico: new potassium-argon ages: Earth and Planetary Science Letters, v. 51, p. 309–321.

Bankey, V., Grauch, V.J.S., Drenth, B.J., and EDCON-PRJ Inc., 2007, Digital data from the Taos West aeromagnetic survey in Taos County, New Mexico: U.S. Geological Survey Open-File Report 2007-1248, 4 p.

Barker, F., 1958, Precambrian and Tertiary geology of Las Tablas quadrangle, New Mexico: New Mexico Bureau of Geology and Mineral Resources Bulletin 45, 104 p.

Bauer, P.W., 1993, Proterozoic tectonic evolution of the Picuris Mountains, northern New Mexico: Journal of Geology, v. 101, p. 483–500.

Bauer, P.W., and Kelson, K.I., 1997 (last revised March 13, 2006), Geologic map of the Taos SW 7.5-minute quadrangle, Taos County, New Mexico: New Mexico Bureau of Geology and Mineral Resources Open-file Geologic Map 12, scale 1:24,000.

Bauer, P.W., and Kelson, K.I., 2004, Rift extension and fault slip rates in the southern San Luis Basin, New Mexico, in Brister, B.S., Bauer, P.W., Read, A.S., and Lueth, V.W., eds., Geology of the Taos Region: New Mexico Geological Society, 55th Annual Field Conference, Guidebook, p. 172–180.

Bauer, P., Kelson, K., Lyman, J., Heynecamp, M., and McCraw, D., 2000, Geologic map of the Rancho de Taos quadrangle, Taos, County, New Mexico: New Mexico Bureau of Geology and Mineral Resources Open-File Geologic Map 33, scale 1:124,000.

Bauer, P.W., Read, A.S., Kelson, K.I., Muehlberger, W.R., and Koning, D.J., 2004, The flanks of the rift, second-day road log from Taos to Taos Pueblo, Llano Quemado, Pilar, and return to Taos, in Brister, B.S., Bauer, P.W., Read, A.S., and Lueth, V.W., eds., Geology of the Taos Region: New Mexico Geological Society, 55th Annual Field Conference, Guidebook, p. 37–75.

Butler, A.P., Jr., 1946, Tertiary and Quaternary geology of the Tusas–Tres Piedras area, New Mexico [Ph.D. dissertation]: Cambridge, Harvard University, 188 p.

Butler, A.P., Jr., 1971, Tertiary volcanic stratigraphy of the eastern Tusas Mountains, southwest of the San Luis Valley, Colorado-New Mexico, in James, H.L., ed., San Luis Basin: New Mexico Geological Society, 22nd Annual Field Conference, Guidebook, p. 289–300.

Cather, S.M., Chamberlin, R.M., Chapin, C.E., and McIntosh, W.C., 1994, Stratigraphic consequences of episodic extension in the Lemitar Mountains, central Rio Grande rift, in Keller, G.R., and Cather, S.M., eds., Basins of the Rio Grande Rift: Structure, Stratigraphy, and Tectonic Setting: Boulder, Colorado, Geological Society of America Special Paper 291, p. 157–169.

Chamberlin, R.M., 1999, Geologic map of the Socorro quadrangle: New Mexico Bureau of Geology and Mineral Resources Open-File Geologic Map 034, scale 1:24,000.

Chamberlin, R.M., Cather, S.M., Nyman, M.W., McLemore, V.T., 2001, Geologic map of the Lemitar quadrangle, Socorro County, New Mexico: New Mexico Bureau of Geology and Mineral Resources Open-File Geologic Map 038, scale 1:24,000.

Chapin, C.E., 2008, Interplay of oceanographic and paleoclimate events with tectonism during middle to late Miocene sedimentation across the southwestern USA: Geosphere, v. 4, no. 6, p. 976–991; doi: 10.1130/GES00171.1.

Chapin, C.E. and Cather, S.M., 1994, Tectonic setting of the axial basins of the northern and central Rio Grande rift, in Keller, G.R., and Cather, S.M., eds., Basins of the Rio Grande Rift: Structure, Stratigraphy, and Tectonic Setting: Boulder, Colorado, Geological Society of America, Special Paper 291, p. 5–25.

Connell, S.D., Hawley, J.W., and Love, D.W., 2005, Late Cenozoic drainage development in the southeastern Basin and Range of New Mexico, southeasternmost Arizona, and western Texas, in Lucas, S.G., Morgan, G.S., and Zeigler, K.E., eds., New Mexico's Ice Ages: Albuquerque, New Mexico, New Mexico Museum of Natural History and Science, Bulletin No. 28, p. 125–150.

Connell, S.D., Smith, G.A., and Mack, G.H., 2012, Evolution of the Rio Grande by fluvial spillover: Abstracts with Programs—Geological Society of America, v. 44, issue 6, p. 14.

Cordell, L., 1979, Gravimetric expression of graben faulting in Santa Fe country and the Española Basin, New Mexico, in Ingersoll, R.V., Woodward, L.A., and James, H.L., eds., Guidebook of Santa Fe Country: New Mexico Geological Society, 30th Annual Field Conference, Guidebook: p. 59–64.

Dethier, D.P., and Reneau, S.L., 1995, Quaternary history of the western Española basin, New Mexico: New Mexico Geological Society, 46th Annual Field Conference, Guidebook, p. 289–298.

Drakos, P., Lazarus, J., Riesterer, J., White, B., Banet, V., Hodgins, M., and Sandoval, J., 2004, Subsurface stratigraphy in the southern San Luis Basin, New Mexico, in Brister, B.S., Bauer, P.W., Read, A.S., and Lueth, V.W., eds., Geology of the Taos Region: New Mexico Geological Society, 55th Fall Field Conference Guidebook, p. 374–382.

Dungan, M.A., Muehlberger, W.R., Leininger, L., Peterson, C., McMillan, N.J., Gunn, G., Lindstrom, M., and Haskin, L., 1984, Volcanic and sedimentary stratigraphy of the Rio Grande gorge and the late Cenozoic evolution of the southern San Luis Valley, in Baldridge, W.S., Dickerson, P.W., Riecker, R.E., and Zidek, J., eds., Rio Grande Rift: Northern New Mexico: New Mexico Geological Society, 35th Annual Field Conference, Guidebook, p. 157–170.

Ebinger, C.J., Van Wijk, J., and Keir, D., 2013, The time scales of continental rifting: Implications for global processes, in Bickford, M.E., ed., The Web of Geological Sciences: Advances, Impacts, and Interactions: Geological Society of America, Special Paper 500, p. 1–26, doi: 10.1130/2013.2500(11).

Ferguson, J.F., Baldridge, W.S., Braile, L.W., Biehler, S., Gilpin, B., and Jiracek, G.R., 1995, Structure of the Española Basin, Rio Grande Rift, New Mexico, from SAGE seismic and gravity data, in Bauer, P.W., Kues, B.S., Dunbar, N.W., Karlstrom, K.E., and Harrison, B., eds., Geology of the Santa Fe Region: New Mexico Geological Society, 46th Annual Field Conference, Guidebook, p. 105–110.

Fleck, R.J., Sutter, J.F., and Elliot, D.H., 1977, Interpretation of discordant 40Ar/39Ar age-spectra of Mesozoic tholeiites from Antarctica: Geochimica et Cosmochimica Acta, v. 41, p. 15–32.

Galusha, T., and Blick, J.C., 1971, Stratigraphy of the Santa Fe Group, New Mexico: Bulletin of the American Museum of Natural History, v. 144, 127 p.

Grauch, V.J.S., and Keller, G.R., 2004, Gravity and aeromagnetic expression of tectonic and volcanic elements of the southern San Luis Basin, New Mexico and Colorado, in Brister, B.S., Bauer, P.W., Read, A.S., and Lueth, V.W., eds., Geology of the Taos Region: New Mexico Geological Society, 55th Annual Field Conference, Guidebook, p. 230–243.

Grauch, V.J.S., and Hudson, M.R., 2007, Guides to understanding the aeromagnetic expression of faults in sedimentary basins: Lessons learned from the central Rio Grande Rift, New Mexico: Geosphere, v. 3, no. 6, p. 596–623. doi: 10.1130/GES00128.1.

Grauch, V.J.S., Bauer, P.W., and Kelson, K.I., 2004, Preliminary interpretation of high-resolution aeromagnetic data collected near Taos, New Mexico, in Brister, B.S., Bauer, P.W., Read, A.S., and Lueth, V.W., eds., Geology of the Taos Region: New Mexico Geological Society, 55th Annual Field Conference, Guidebook 55, p. 244–256.

Grauch, V.J.S., Sawyer, D.A., Minor, S.A., Hudson, M.R., and Thompson, R.A., 2006, Gravity and aeromagnetic studies of the Santo Domingo Basin area, New Mexico (Chapter D), in Minor, S.A., ed., The Cerrillos uplift, the La Bajada Constriction, and hydrogeologic framework of the Santo Domingo Basin, Rio Grande rift: U.S. Geological Survey Professional Paper 1720, p. 61–86.

Just, E., 1937, Geology and economic features of the pegmatites of Taos and Rio Arriba Counties, New Mexico: New Mexico Bureau of Geology and Mineral Resources Bulletin 13, 73 p.

Kelley, V.C., 1978, Geology of the Española Basin, New Mexico: New Mexico Bureau of Mines and Mineral Resources Geologic Map 48, scale 1:125,000.

Kelson, K.I., and Bauer, P.W., 1998 (last modified 09 March 2006), Geologic map of the Carson quadrangle, Taos County, New Mexico: New Mexico Bureau of Geology and Mineral Resources Open-file Geologic Map 22, scale 1:24,000.

Kelson, K.I., Bauer, P.W., Diehl, K.S., Shapo, D., 2001 (last revised March 15, 2006), Geologic map of the Taos quadrangle, Taos County, New Mexico: New Mexico Bureau of Geology and Mineral Resources Open-File Geologic Map 43, scale 1:24,000.

Kelson, K.I., Bauer, P.W., Unruh, J.R., and Bott, J.D.J., 2004, Late Quaternary characteristics of the northern Embudo fault, Taos County, New Mexico, in Brister, B.S., Bauer, P.W., Read, A.S., and Lueth, V.W., eds., Geology of the Taos Region: New Mexico Geological Society, 55th Annual Field Conference, Guidebook, p. 147–157.

Koning, D.J., 2004, Geologic map of the Lyden 7.5-minute quadrangle, Rio Arriba and Santa Fe counties, New Mexico: New Mexico Bureau of Geology and Mineral Resources Open-File Geologic Map 83, scale 1:24,000.

Koning, D.J., and Aby, S., 2003, revised June-2004, Geologic map of the Velarde 7.5-minute quadrangle, Rio Arriba and Taos counties, New Mexico: New Mexico Bureau of Geology and Mineral Resources Open-File Geologic Map, scale 1:24,000.

Koning, D.J., and Aby, S.B., 2005, Proposed members of the Chamita Formation, north-central New Mexico, in Lucas, S.G., Zeigler, K.E., Lueth, V.W., and Owen, D.E., eds., Geology of the Chama Basin: New Mexico Geological Society, 56th Annual Field Conference, Guidebook, p. 258–278.

Koning, D.J., and Manley, K., 2003, last-modified September 2014, Geologic map of the San Juan Pueblo 7.5-minute quadrangle, Rio Arriba and Santa Fe Counties, New Mexico: New Mexico Bureau of Geology and Mineral Resources Open-File Geologic Map 70, scale 1:24,000.

Koning, D.J., and Mansell, M.M., 2011, Plate 2, Regional Geologic Map of North-central New Mexico, in Koning, D.J., Karlstrom, K.E., Kelley, S.A., Lueth, V.W., and Aby, S.B., eds., Geology of the Tusas Mountains and Ojo Caliente Area: New Mexico Geological Society, 62nd Annual Field Conference, Guidebook, p. 150.

Koning, D.J., Ferguson, J.F., Paul, P.J., and Baldridge, W.S., 2004a, Geologic structure of the Velarde graben and southern Embudo fault system, north-central N.M., in Brister, B.S., Bauer, P.W., Read, A.S., and Lueth, V.W., eds., Geology of the Taos Region: New Mexico Geological Society, 55th Annual Field Conference, Guidebook, p. 158–171.

Koning, D.J., Aby, S.B., and Dunbar, N., 2004b, Middle-upper Miocene stratigraphy of the Velarde graben, north-central New Mexico: Tectonic and paleogeographic implications, in Brister, B.S., Bauer, P.W., Read, A.S., and Lueth, V.W., eds., Geology of the Taos Region: New Mexico Geological Society, 55th Annual Field Conference, Guidebook, p. 359–373.

Koning, D.J., Aby, S., and Kelson, K., 2007a, Preliminary geologic map of the Taos Junction quadrangle, Taos County, New Mexico: New Mexico Bureau of Geology and Mineral Resources Open-File Geologic Map 144, scale 1:24,000.

Koning, D.J., Karlstrom, K.E., Salem, A., and Lombardi, C., 2007b, Preliminary geologic map of the La Madera quadrangle, Rio Arriba County, New Mexico: New Mexico Bureau of Geology and Mineral Resources Open-File Geologic Map 141, scale 1:12,000.

Koning, D.J., McIntosh, W., and Dunbar, N., 2011, Geology of southern Black Mesa, Española Basin, New Mexico: new stratigraphic age control and interpretation of the southern Embudo fault system of the Rio Grande rift, in Koning, D.J., Karlstrom, K.E., Kelley, S.A., Lueth, V.W., and Aby, S.B., eds., Geology of the Tusas Mountains and Ojo Caliente Area: New Mexico Geological Society, 62nd Annual Field Conference, Guidebook, p. 191–214.

Koning, D.J., Grauch, V.J.S., Connell, S.D., Ferguson, J., McIntosh, W., Slate, J.L., Wan., E., and Baldridge, W.S., 2013, Structure and tectonic evolution of the eastern Española Basin, Rio Grande rift, north-central New Mexico, in Hudson, M., and Grauch, V.J.S., eds., New Perspectives on the Rio Grande rift: From Tectonics to Groundwater: Geological Society of America, Special Paper 494, p. 185–219, doi:10.1130/2013.2494(08).

Koning, D.J., Aby, S.B., Jochems, A.P., Chamberlin, R.M., Lueth, W.V., and Peters, L., 2015, Relating ca. 5 Ma coarse sedimentation in the Rio Grande rift to tectonics, climate, and inter-basin fluvial spillover of the ancestral Rio Grande: Proceedings Volume, 2015 Annual Spring Meeting of the New Mexico Geological Society, p. 28: http://nmgs.nmt.edu/meeting/2015/Spring_Meeting_Program_2015.pdf (accessed October 2015).

Koning, D.J., Jochems, A.P., Morgan, G.S., Lueth, W.V., and Peters, L., 2016a, Stratigraphy, gravel provenance, and age of early Rio Grande deposits exposed 1–2 km northwest of downtown Truth or Consequences, New Mexico, in Frey, B.A., Lucas, S.G., Williams, S., Zeigler, K.E., McLemore, V.T., Karlstrom, K.E, and Ulmer-Scholle, D.S., eds., Belen area: New Mexico Geological Society, 67th Annual Field Conference (in press).

Koning, D.J., WoldeGabriel, G., and Broxton, D.E., 2016b, Stratigraphy and age control bracketing the early development of the paleo-Rio Chama: Proceedings Volume, 2016 Annual Spring Meeting of the New Mexico Geological Society, p. 35: http://nmgs.nmt.edu/meeting/2016/Spring_Meeting_Program_2016.pdf (accessed May 2016).

Kottlowski, 1953, Tertiary-Quaternary sediments of the Rio Grande Valley in southern New Mexico, in Kottlowski, F.E., ed., Southwestern New Mexico: New Mexico Geological Society, 4th Annual Field Conference, Guidebook, p. 144–148.

Kuiper, K.F., Deino, A., Hilgen, F.J., Krijgsman, W., Renne, P.R., and Wijbrans, J.R., 2008, Synchronizing rock clocks in Earth history: Science, v. 320, p. 500–504.

Lambert, W., 1966, Notes on the late Cenozoic geology of the Taos-Questa area, New Mexico, in Northrop, S.A., and Read, C.B., eds., Taos-Raton-Spanish Peaks Country (New Mexico and Colorado: New Mexico Geological Society, 17th Annual Field Conference, Guidebook, p. 43–50.

Lipman, P.W., and Mehnert, H.H., 1979, The Taos Plateau volcanic field, northern Rio Grande rift, New Mexico, in Riecker, R.E., ed., Rio Grande rift,: Tectonics and Magmatism: Washington, D.C., American Geophysical Union, p. 289–311.

Lipman, P.W., and Reed, J.C. Jr., 1989, Geologic map of the Latir Volcanic Field and adjacent areas, northern New Mexico: U.S. Geological Survey Miscellaneous Investigation Series Map I-1907, scale 1:48,000.

Lipman, P.W., Mehnert, H.H., and Naeser, C.W., 1986, Evolution of the Latir volcanic field, northern New Mexico, and its relation to the Rio Grande Rift, as indicated by potassium-argon and fission track dating: Journal of Geophysical Research, v. 91, issue B6, p. 6329–6345.

Machette, M.N., Thompson, R.A., Marchetti, D.W., and Smith, R.S.U., 2013, Evolution of Lake Alamosa and integration of the Rio Grande during the Pliocene and Pleistocene, in Hudson, M., and Grauch, V.J.S., eds., New Perspectives on the Rio Grande rift: From Tectonics to Groundwater: Geological Society of America, Special Paper 494, p. 1–20, doi:10.1130/2013.2494(01).

Mack, G.H., Love, D.W., and Seager, W.R., 1997, Spillover models for axial rivers in regions of continental extension: The Rio Mimbres and Rio Grande in the southern Rio Grande rift, USA: Sedimentology, v. 44, p. 637–652.

Mack, G.H., Salyards, S.L., McIntosh, W.C., and Leeder, M.R., 1998, Reversal magnetostratigraphy and radioisotopic geochronology of the Plio-Pleistocene Camp Rice and Palomas formations, southern Rio Grande rift, in Mack, G.H., Austin, G.S., and Barker, J.M., eds., Las Cruces Country II: New Mexico Geological Society, 49th Annual Field Conference, Guidebook, p. 229–236.

Mack, G.H., Seager, W.R., Leeder, M.R., Perez-Arlucea, M., and Salyards, S.L., 2006, Pliocene and Quaternary history of the Rio Grande, the axial river of the southern Rio Grande rift, New Mexico, USA: Earth-Science Reviews, v. 79, p. 141–162.

Maldonado, F., and Miggins, D.P., 2007, Geologic summary of the Abiquiu quadrangle, north-central New Mexico, in Kues, B.S., Kelley, S.A., and Lueth, V.W., eds., Geology of the Jemez Region II: New Mexico Geological Society Guidebook, 58th Annual Field Conference, Guidebook, p. 182–187.

Maldonado, F., and Kelley, S.A., 2009, Revisions to the stratigraphic nomenclature of the Abiquiu Formation, Abiquiu and contiguous areas, north-central New Mexico: New Mexico Geology, v. 31, p. 3–8.

Maldonado, F., Miggins, D.P., Budahn, J.R., and Spell, T., 2013, Deformational and erosional history for the Abiquiu and contiguous area, north-central New Mexico, in Hudson, M.R., and Grauch, V.J.S., eds., New Perspectives on Rio Grande Rift Basins: From Tectonics to Groundwater: Geological Society of America Special Paper 494, p. 125–155. doi: 10.1130/2013.2494(06).

Manley, K., 1976, The Late Cenozoic History of the Española Basin, New Mexico [Ph.D. thesis]: Boulder, University of Colorado, 1–171 p.

Manley, K., 1979a, Stratigraphy and structure of the Española basin, Rio Grande rift, New Mexico, in Riecker, R.E., ed., Rio Grande rift,: Tectonics and Magmatism: Washington, D.C., American Geophysical Union, p. 71–86.

Manley, K., 1979b, Tertiary and Quaternary stratigraphy of the Northeast Plateau, Española Basin, New Mexico, in Ingersoll, R.V., Woodward, LA., and James, H.L., eds., Guidebook of Santa Fe Country: New Mexico Geological Society, 30th Annual Field Conference, Guidebook, p. 231–236.

Manley, I., 1981, Redefinition and description of the Los Pinos Formation of north-central New Mexico: Geological Society of America Bulletin, Part I, v. 92, p. 984–989.

May, J., 1980, Neogene geology of the Ojo Caliente–Rio Chama area, Española Basin, New Mexico [Ph.D. thesis]: Albuquerque, New Mexico, University of New Mexico, 204 p.

McIntosh, W.C., Heizler, M., Peters, L., Esser, R., 2003, 40Ar/39Ar Geochronology at the New Mexico Bureau of Geology and Mineral Resources: Open-File Report OF-Ar-1, 10p.

McIntosh, W.C., Koning, D.J., and Zimmerer, M., 2011, Irregular bodies of non-welded Amalia tuff within the Peña Tank Rhyolite, western San Luis Basin, north-central New Mexico in Koning, D.J., Karlstrom, K.E., Kelley, S.A., Lueth, V.W., and Aby, S.B., eds., Geology of the Tusas Mountains and Ojo Caliente Area: New Mexico Geological Society, 62nd Annual Field Conference, Guidebook, p. 223–234.

Montgomery, A., 1953, Precambrian geology of the Picuris Range, north-central New Mexico: New Mexico Bureau of Mines and Mineral Resources Bulletin 30, 89 p.

Muehlberger, W.R., 1978, Frontal fault zone of northern Picuris Range, in Hawley, J., compiler, Guidebook to Rio Grande rift in New Mexico and Colorado: New Mexico Bureau of Mines and Mineral Resources, Circular 163, p. 44–45.

Muehlberger, W.R., 1979, The Embudo fault between Pilar and Arroyo Hondo, New Mexico -- An active intracontinental transform fault, in Ingersoll, R.V., Woodward, L.A., and James, H.L., eds., Santa Fe Country: New Mexico Geological Society, 30th Annual Field Conference, Guidebook, p. 77–82.

Nier, A.O., 1950, A redetermination of the relative abundances of the isotopes of carbon, nitrogen, oxygen, argon, and potassium: Physical Review Letters, v. 77, 789–793.

NMBGMR (New Mexico Bureau of Geology and Mineral Resources), 2003, Geologic Map of New Mexico: New Mexico Bureau of Geology and Mineral Resources, published in cooperation with the U.S. Geological Survey, scale 1:500,000.

Ogg, J.G., 2012, Geomagnetic polarity time scale, in Gradstein, F.M., Ogg, J.G., Schmitz, M.D., and Ogg, G.M., eds., The Geologic Time Scale 2012, p. 31–42.

Ozima, A., Kono, M., Kaneoka, I., Kinoshita, H., Nagata, T., Larson, E.E., and Strangway, D.W., 1967, Paleomagnetism and potassium-argon ages of some volcanic rocks from the Rio Grande gorge, New Mexico: Journal of Geophysical Research, v. 72, p. 2615-2622.

Pazzaglia, F.J., and Wells, S.G., 1990, Quaternary stratigraphy, soils and geomorphology of the northern Rio Grande rift, in Bauer, P.W., Lucas, S.G., Mawer, C.K., and McIntosh, eds., Tectonic Development of the Southern Sangre de Cristo Mountains: New Mexico Geological Society, 41st Annual Fall Field Conference, Guidebook, p. 423–430.

Rehder, T.R., 1986, Stratigraphy, sedimentology, and petrography of the Picuris Formation in Ranchos de Taos and Tres Rito quadrangles, north-central New Mexico [M.S. thesis]: Dallas, Southern Methodist Universtiy, 110 p.

Repasch, M., Karlstrom, K., and Heizler, M., 2015a, Neotectonic influences on the evolution of the Rio Grande fluvial system over the last 5 Ma: Geological Society of America Abstracts with Programs, v. 44, issue 6, p. 14, v. 47, no. 7, p. 551.

Repasch, M., Karlstrom, K., and Heizler, M., 2015b, Birth and evolution of the Rio Grande-Rio Chama fluvial system: The influence of magma-driven dynamic topography on fluvial systems over the last 8 Ma: Abstract EP41A-0912 presented at 2015 Fall Meeting, AGU, San Francisco, California, December.

Smith, G.A., 2004, Middle to late Cenozoic development of the Rio Grande rift and adjacent regions in northern New Mexico, in Mack, G.H., and Giles, K.A., eds., The Geology of New Mexico, A Geologic History: New Mexico Geological Society, Special Publication 11, p. 331–358.

Smith, G.A., McIntosh, W., and Kuhle, A.J., 2001, Sedimentologic and geomorphic evidence for seesaw subsidence of the Santo Domingo accommodation-zone basin, Rio Grande rift, New Mexico: Geologic Society of America Bulletin, v. 113, no. 5, p. 561–574.

Spiegel, Z., and Baldwin, B., 1963, Geology and Water Resources of the Santa Fe Area, New Mexico: Washington, D.C., Geological Survey Water-Supply Paper 1525, 258 p.

Steinpress, M.G., 1981, Neogene stratigraphy and structure of the Dixon area, Española basin, north-central New Mexico: Geological Society of America Bulletin, v. 92, p. 1023–1026.

Thompson, R.A., and McMillan, N.J., 1992, A geologic overview and one-day field guide of the Taos Plateau volcanic field, Taos County, New Mexico: U.S. Geological Survey Open-File Report 92-528, 23 p.

U.S. Geological Survey, 2009, Water-Data Report, 082900000 Rio Chama near Chamita, NM: http://wdr.water.usgs.gov/wy2009/pdfs/08290000.2009.pdf (last accessed January 13, 2016).

Appendices

Available in Data Repository 20160002

http://geoinfo.nmt.edu/repository/index.cfml?rid=20160002

Appendix 1. $^{40}Ar/^{39}Ar$ data tables and analytical parameters.

Appendix 2. Descriptions of stratigraphic units predating and postdating the Sandlin unit.

Appendix 3. Detailed descriptions and photographs of the north, middle, and south Cerro Azul stratigraphic sections.

Appendix 4. Outcrop descriptions for the upper Sandlin unit near U.S. Highway 285.

Appendix 5. Clast count data (raw data and percentages).

Appendix 6. Tabulation of paleoflow data for the Sandlin unit.

Appendix 7. Age spectrums and isochron plots for three samples from Appelt (1998).